Interventions targeting nonsymptomatic cases can be important to prevent local outbreaks: SARS-CoV-2 as a case-study

Authors

Francesca A. Lovell-Read[1*], Sebastian Funk[2], Uri Obolski[3,4], Christl A. Donnelly[5,6], Robin N. Thompson[1,2,7,8]

Affiliations

[1]Mathematical Institute, University of Oxford, Oxford, UK

[2]Centre for Mathematical Modelling of Infectious Diseases, London School of Hygiene & Tropical Medicine, London, UK

[3]Porter School of the Environment and Earth Sciences, Tel Aviv University, Tel Aviv, Israel

[4]School of Public Health, Tel Aviv University, Tel Aviv, Israel

[5]Department of Statistics, University of Oxford, Oxford, UK

[6]MRC Centre for Global Infectious Disease Analysis, Department of Infectious Disease Epidemiology, Imperial College London, London, UK

[7]Mathematics Institute, University of Warwick, Coventry, UK

[8]The Zeeman Institute for Systems Biology and Infectious Disease Epidemiology Research, University of Warwick, Coventry, UK

*** Corresponding author**

Address: Merton College, Merton Street, Oxford, OX1 4JD

E-mail: francesca.lovell-read@merton.ox.ac.uk. Tel: +44 (0)7511 676 592.

Abstract

During infectious disease epidemics, an important question is whether cases travelling to new locations will trigger local outbreaks. The risk of this occurring depends on the transmissibility of the pathogen, the susceptibility of the host population and, crucially, the effectiveness of surveillance in detecting cases and preventing onward spread. For many pathogens, transmission from presymptomatic and/or asymptomatic (together referred to as nonsymptomatic) infectious hosts can occur, making effective surveillance challenging. Here, using SARS-CoV-2 as a case-study, we show how the risk of local outbreaks can be assessed when nonsymptomatic transmission can occur. We construct a branching process model that includes nonsymptomatic transmission, and explore the effects of interventions targeting nonsymptomatic or symptomatic hosts when surveillance resources are limited. We consider whether the greatest reductions in local outbreak risks are achieved by increasing surveillance and control targeting nonsymptomatic or symptomatic cases, or a combination of both. We find that seeking to increase surveillance of symptomatic hosts alone is typically not the optimal strategy for reducing outbreak risks. Adopting a strategy that combines an enhancement of surveillance of symptomatic cases with efforts to find and isolate nonsymptomatic infected hosts leads to the largest reduction in the probability that imported cases will initiate a local outbreak.

Keywords

mathematical modelling; infectious disease epidemiology; SARS-CoV-2; COVID-19; presymptomatic infection; asymptomatic infection; disease surveillance

1. Introduction

Emerging epidemics represent a substantial challenge to human health worldwide [1-4]. When cases are clustered in specific locations, two key questions are: i) Will exported cases lead to local outbreaks in new locations? and ii) Which surveillance and control strategies in those new locations will reduce the risk of local outbreaks?

Branching process models are used for a range of diseases to assess whether cases that are newly arrived in a host population will generate a local outbreak driven by sustained local transmission [5-11]. These models can also be used to predict the effectiveness of potential control interventions. For example, early in the COVID-19 pandemic, Hellewell *et al.* [12] used simulations of a branching process model to predict whether or not new outbreaks would fade out under different contact tracing strategies. Thompson [13] estimated the probability of local outbreaks analytically using a branching process model and found that effective isolation of infectious hosts leads to a substantial reduction in the outbreak risk.

A factor that can hinder control interventions during any epidemic is the potential for individuals to transmit a pathogen while not showing symptoms. For COVID-19, the incubation period has been estimated to last approximately five or six days on average [14, 15], and presymptomatic transmission can occur during that period [16-20]. Additionally, asymptomatic infected individuals (those who never develop symptoms) are also thought to contribute to transmission [16, 21, 22].

Motivated by the need to assess the risk of outbreaks outside China early in the COVID-19 pandemic, we show how the risk that imported cases will lead to local outbreaks can be estimated using a branching process model. Unlike standard approaches for estimating the probability of a major epidemic analytically [23-26], nonsymptomatic individuals are included in the model

explicitly. Using a function that characterises the efficacy of interventions for different surveillance efforts (denoted $f(\rho, \delta)$ in the model), we explore the effects of interventions that aim to reduce this risk. Under the assumption that detected infected hosts are isolated effectively, we consider whether it is most effective to dedicate resources to enhancing surveillance targeting symptomatic individuals, to instead focus on increasing surveillance for nonsymptomatic individuals, or to use a combination of these approaches.

We show that, when surveillance resources are limited, the maximum reduction in the outbreak risk almost always corresponds to a mixed strategy involving enhanced surveillance of both symptomatic and nonsymptomatic hosts. This remains the case even if the surveillance effort required to find nonsymptomatic infected individuals is significantly larger than the effort required to find symptomatic individuals. This highlights the benefits of not only seeking to find and isolate symptomatic hosts, but also dedicating resources to detecting nonsymptomatic cases during infectious disease epidemics.

2. Methods

2.1 Model

We consider a branching process model in which infectious individuals are classified as asymptomatic (A), presymptomatic (I_1) or symptomatic (I_2). Hosts in any of these classes may generate new infections. The parameter ξ represents the proportion of new infections that are asymptomatic, so that a new infection either involves increasing A by one (with probability ξ) or increasing I_1 by one (with probability $1 - \xi$).

Presymptomatic hosts may go on to develop symptoms (transition from I_1 to I_2) or be detected and isolated (so that I_1 decreases by one). Symptomatic individuals (I_2) can be isolated (so that I_2 decreases by one) or be removed due to recovery or death (so that again I_2 decreases by one). Similarly, asymptomatic hosts may be detected and isolated, or recover (so that A decreases by one in either case).

A schematic showing the different possible events in the model is shown in Fig 1A. The analogous compartmental differential equation model to the branching process model that we consider is given by

$$\frac{\mathrm{d}A}{\mathrm{d}t} = \xi(\eta\beta A + \alpha\beta I_1 + \beta I_2) - \frac{\varepsilon\gamma}{1 - \mathrm{f}(\rho_1, \delta)} A - \nu A,$$

$$\frac{\mathrm{d}I_1}{\mathrm{d}t} = (1 - \xi)(\eta\beta A + \alpha\beta I_1 + \beta I_2) - \frac{\varepsilon\gamma}{1 - \mathrm{f}(\rho_1, \delta)} I_1 - \lambda I_1,$$

$$\frac{\mathrm{d}I_2}{\mathrm{d}t} = \lambda I_1 - \frac{\gamma}{1 - \mathrm{f}(\rho_2, \delta)} I_2 - \mu I_2.$$

The parameters of the model, and the form of the function $f(\rho, \delta)$ that describes how the expected time to isolation is reduced for a given surveillance effort, are outlined below.

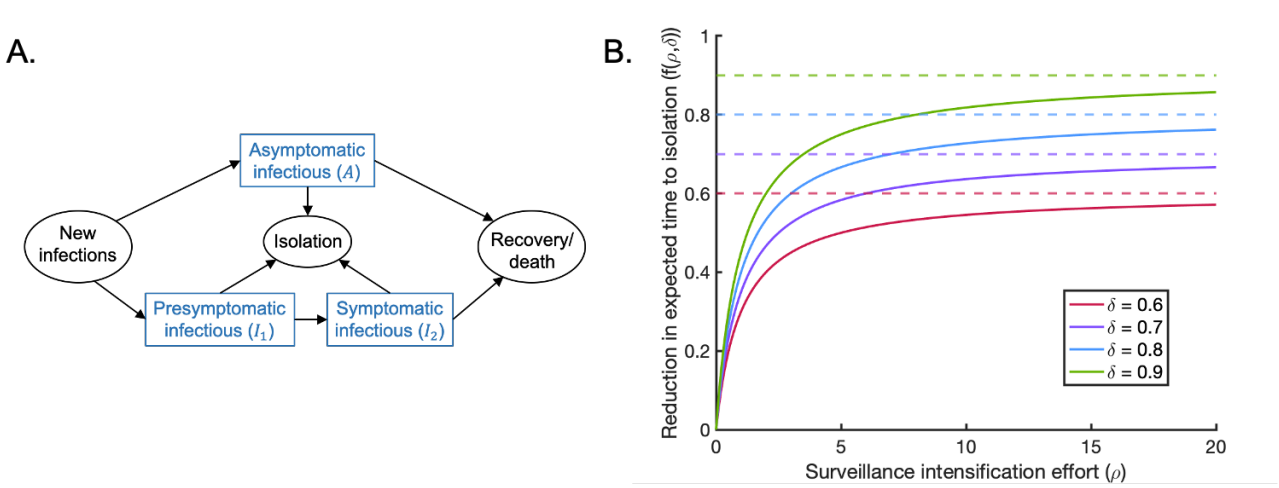

Fig 1. The branching process model used in our analyses. A. Schematic showing the different event types in the branching process model. The parameters of the model are described in the text and in Table 1. B. The relationship between the surveillance intensification effort (ρ) and the proportional reduction in the expected time to isolation ($f(\rho, \delta)$), shown for different values of the parameter δ (solid lines). The parameter $\delta \in (0,1)$ represents the upper bound of $f(\rho, \delta)$ (dotted lines). This general functional relationship between surveillance effort and isolation effectiveness is assumed to hold for surveillance of both nonsymptomatic and symptomatic individuals, although nonsymptomatic hosts are more challenging to detect than symptomatic hosts ($\varepsilon < 1$).

In our model, the parameter β and its scaled counterparts $\alpha\beta$ and $\eta\beta$ represent the rates at which symptomatic, presymptomatic and asymptomatic hosts generate new infections, respectively. Since we are modelling the beginning of a potential local outbreak, we assume that the size of the susceptible population remains approximately constant and do not track the depletion of this population. The parameter λ governs the rate at which presymptomatic individuals develop symptoms, so that the expected duration of the presymptomatic period is $1/\lambda$ days in the absence of interventions. Similarly, without interventions, the expected durations of the symptomatic and asymptomatic infectious periods are $1/\mu$ days and $1/\nu$ days, respectively.

The baseline rate at which symptomatic individuals are detected and isolated is determined by the parameter γ. Assuming that nonsymptomatic individuals are more difficult to detect than symptomatic individuals, we take the analogous quantity for nonsymptomatic hosts to be $\varepsilon\gamma$, where the scaling factor $\varepsilon < 1$ reflects the fact that interventions targeting nonsymptomatic hosts are likely to be less effective for the same surveillance effort. We assume that the sensitivity of surveillance is identical for presymptomatic and asymptomatic individuals, and therefore use the same isolation rate for both of these groups.

The parameters ρ_1 and ρ_2 represent the surveillance intensification effort targeted at nonsymptomatic and symptomatic hosts, respectively. The function $f(\rho, \delta) = \frac{\delta\rho}{1+\rho}$ governs the proportional reduction in the expected time to isolation for a given surveillance effort, ρ (for a similar approach in which the proportion of infectious cases prevented is assumed to be a function of control effort, see Matthews *et al.* [27]). The functional form of $f(\rho, \delta)$ is chosen for three main reasons. First, it generates a reduced expected time to isolation when the surveillance effort increases. Second, since the proportional reduction in the expected time to isolation is bounded above by the parameter $\delta \in (0,1)$, the isolation rate saturates and cannot increase indefinitely. Third, the gradient $\frac{\partial f}{\partial \rho}$ decreases with the surveillance effort ρ, meaning that an increase in the surveillance effort has a greater impact at low surveillance efforts compared to when this effort is already large [27]. The function $f(\rho, \delta)$ is shown in Fig 1B for different values of the parameter δ.

2.2 Reproduction number

The basic reproduction number, R_0, represents the expected number of secondary infections generated by a single infected individual introduced at the start of their infection into a fully susceptible population in the absence of intensified surveillance:

$$R_0 = \frac{\xi\eta\beta}{\nu + \epsilon\gamma} + (1 - \xi)\left[\frac{\alpha\beta}{\lambda + \epsilon\gamma} + \frac{\lambda}{\lambda + \epsilon\gamma}\frac{\beta}{\gamma + \mu}\right].$$

This expression is the sum of the expected number of transmissions from a host who begins in the asymptomatic class and from a host who begins in the presymptomatic infectious class, weighted by the respective probabilities ξ and $1 - \xi$ that determine the chance that the host experiences a fully asymptomatic course of infection. The expected number of transmissions from a host who begins in the presymptomatic infectious class comprises transmissions occurring during the

incubation period and transmissions occurring during the symptomatic period, accounting for the possibility that the host is isolated prior to developing symptoms.

The proportion of infections arising from presymptomatic hosts in the absence of intensified surveillance is then given by

$$K_p = \frac{\frac{(1-\xi)\alpha}{\lambda+\epsilon\gamma}}{\frac{\xi\eta}{\nu+\epsilon\gamma} + (1-\xi)\left[\frac{\alpha}{\lambda+\epsilon\gamma} + \frac{\lambda}{\lambda+\epsilon\gamma}\frac{1}{\gamma+\mu}\right]}, \quad (1)$$

and the equivalent quantity for asymptomatic hosts is given by

$$K_a = \frac{\frac{\xi\eta}{\nu+\epsilon\gamma}}{\frac{\xi\eta}{\nu+\epsilon\gamma} + (1-\xi)\left[\frac{\alpha}{\lambda+\epsilon\gamma} + \frac{\lambda}{\lambda+\epsilon\gamma}\frac{1}{\gamma+\mu}\right]}. \quad (2)$$

2.3 Baseline values of model parameters

Since this research was motivated by the need to estimate outbreak risks outside China in the initial stages of the COVID-19 pandemic, we used a baseline set of parameter values in our analyses that was informed by studies conducted during this pandemic (Table 1). Where possible, these parameter values were obtained from existing literature. However, we also performed sensitivity analyses to determine how our results varied when the parameter values were changed (see Supplementary Text S3 and Supplementary Figs S3-12). In Table 1, and throughout, rounded values are given to three significant figures.

Table 1. Parameters of the model and the values used in the baseline version of our analysis.

Parameter	Meaning	Baseline value	Justification
R_0	Expected number of secondary infections caused by a single	$R_0 = 3$	Within estimated range for SARS-CoV-2 [28-31]

	infected individual (when $\rho_1 = \rho_2 = 0$)		
ξ	Proportion of infections that are asymptomatic	$\xi = 0.2$	[32-34]
β	Rate at which symptomatic individuals generate new infections	$\beta = 0.336$ days^{-1}	Chosen so that $R_0 = 3$
α	Relative infectiousness of presymptomatic individuals compared to symptomatic individuals	$\alpha = 2.78$	Chosen so that 48.9% of transmissions arise from presymptomatic hosts (i.e. $K_p = 0.489$) [16]
η	Relative infectiousness of asymptomatic individuals compared to symptomatic individuals	$\eta = 0.519$	Chosen so that 10.6% of transmissions arise from asymptomatic hosts (i.e. $K_a = 0.106$) [16]
γ	Isolation rate of symptomatic individuals without intensified surveillance	$\gamma = 0.0924$ days^{-1}	Chosen so that $\frac{1}{\gamma+\mu} = 4.6$ days [35]
ε	Relative isolation rate of nonsymptomatic individuals without intensified surveillance (compared to symptomatic individuals)	$\varepsilon = 0.1$	Assumed; chosen within the range $\varepsilon \in (0,1)$ (for different values, see Fig S7)
λ	Rate at which presymptomatic individuals develop symptoms	$\lambda = 0.5$ days^{-1}	[20]
μ	Recovery rate of symptomatic individuals	$\mu = 1/8$ days^{-1}	[36-38]
ν	Recovery rate of asymptomatic individuals	$\nu = 0.1$ days^{-1}	Chosen so that, in the absence of interventions, the expected duration of infection is identical for all infected hosts $\left(\frac{1}{\nu} = \frac{1}{\lambda} + \frac{1}{\mu}\right)$
δ	Upper bound on the fractional reduction in the time to isolation	$\delta = 0.8$	Assumed; chosen within the natural range $\delta \in (0,1)$ (for different values, see Fig S11)
ρ_1	Surveillance intensification effort targeted at nonsymptomatic hosts	ρ_1 allowed to vary in the range [0,20]	N/A – range of values explored
ρ_2	Surveillance intensification effort targeted at symptomatic hosts	ρ_2 allowed to vary in the range [0,20]	N/A – range of values explored

The value of the parameter governing the baseline rate at which symptomatic individuals are isolated, γ, was chosen to match empirical observations which indicate that individuals who seek

medical care prior to recovery or death do so around four to six days after symptom onset [35]. Specifically, we assumed that the period of time to the first medical visit could be used a proxy for the time to isolation, and chose γ so that the expected time period to isolation conditional on isolation occurring during the symptomatic period was given by $\frac{1}{\gamma+\mu} = 4.6$ days [35]. This is different to the time period that we refer to as the expected time to isolation for symptomatic hosts, which is $\frac{1}{\gamma}$ days (see Methods).

2.4 Probability of a local outbreak

For stochastic simulations of compartmental epidemiological models starting from a small number of hosts infected initially, there are generally two qualitatively different types of behaviour. The pathogen may fade out rapidly, or case numbers may begin to increase exponentially (only starting to fade out once the number of susceptible individuals has been sufficiently depleted, unless public health measures are introduced to reduce transmission). Consequently, running many simulations of those types of model with R_0 larger than but not close to one, the epidemic size is distributed bimodally, with the total number of individuals ever infected falling into one of two distinct ranges (for a simple example, see Supplementary Fig S1A; see also [39-41]). In that scenario, a natural definition for the probability of a local outbreak is therefore the proportion of outbreak simulations for which the total number of infected individuals falls into the higher of these two ranges.

Here, since we are considering the initial phase of potential local outbreaks, we instead considered a branching process model in which depletion of susceptibles was not accounted for. If simulations of branching process models are run, then in each simulation the pathogen either fades out with few infections or case numbers generally increase indefinitely. The probability of a local outbreak

starting from a small number of infected hosts then corresponds to the proportion of simulations in which the pathogen does not fade out quickly and case numbers increase indefinitely instead. This again provides a natural definition of a local outbreak, since simulations can be partitioned into two distinct sets (for an example in which simulations of a simple branching process model are used to calculate the probability of a local outbreak, see Supplementary Fig S1B).

As an alternative to repeated simulation, we instead use our branching process model (Fig 1A) to perform analytic calculations of the probability that a single imported infectious host initiates a local outbreak. To do this, we denote the probability of a local outbreak not occurring, starting from i presymptomatic hosts, j symptomatic hosts, and k asymptomatic hosts, by $q_{i,j,k}$. Starting from one presymptomatic host (so that $i = 1$ and $j = k = 0$), there are four possibilities for the next event. That host could:

i) generate a new asymptomatic infection (with probability $\frac{\xi\alpha\beta}{\alpha\beta+\lambda+\frac{\varepsilon\gamma}{1-f(\rho_1,\delta)}}$);

ii) generate a new presymptomatic infection (with probability $\frac{(1-\xi)\alpha\beta}{\alpha\beta+\lambda+\frac{\varepsilon\gamma}{1-f(\rho_1,\delta)}}$);

iii) develop symptoms (with probability $\frac{\lambda}{\alpha\beta+\lambda+\frac{\varepsilon\gamma}{1-f(\rho_1,\delta)}}$), or;

iv) be isolated (with probability $\frac{\frac{\varepsilon\gamma}{1-f(\rho_1,\delta)}}{\alpha\beta+\lambda+\frac{\varepsilon\gamma}{1-f(\rho_1,\delta)}}$).

These probabilities are obtained by considering the rates at which different possible events occur in the branching process model. Presymptomatic hosts generate new infections at rate $\alpha\beta$, and these new infections occur in asymptomatic and presymptomatic hosts with probabilities ξ and $1-\xi$, respectively. Therefore, starting from a single presymptomatic host, new asymptomatic infections occur at rate $\xi\alpha\beta$, whilst new presymptomatic infections occur at rate $(1-\xi)\alpha\beta$.

Additionally, presymptomatic hosts develop symptoms at rate λ, and are isolated at rate $\frac{\epsilon\gamma}{1-f(\rho_1,\delta)}$. The overall rate at which events occur is the sum of these individual event rates:

$$\text{Total event rate} = \alpha\beta + \lambda + \frac{\epsilon\gamma}{1-f(\rho_1,\delta)}.$$

For each of the four possible next events (i-iv, above), the probability that event occurs next is the individual rate at which that event occurs divided by the total event rate, leading to the expressions given.

We use these probabilities to condition on the event that occurs next in the branching process, following the introduction of a single presymptomatic infectious individual into the population. If that event is the generation of a new asymptomatic infection, which occurs with probability $\frac{\xi\alpha\beta}{\alpha\beta+\lambda+\frac{\varepsilon\gamma}{1-f(\rho_1,\delta)}}$, the probability that a local outbreak subsequently does not occur is $q_{1,0,1}$. Applying analogous reasoning to the other possible events, we obtain

$$q_{1,0,0} = \frac{\xi\alpha\beta}{\alpha\beta+\lambda+\frac{\varepsilon\gamma}{1-f(\rho_1,\delta)}} q_{1,0,1} + \frac{(1-\xi)\alpha\beta}{\alpha\beta+\lambda+\frac{\varepsilon\gamma}{1-f(\rho_{1,\delta})}} q_{2,0,0} + \frac{\lambda}{\alpha\beta+\lambda+\frac{\varepsilon\gamma}{1-f(\rho_{1,\delta})}} q_{0,1,0} + \frac{\frac{\varepsilon\gamma}{1-f(\rho_{1,\delta})}}{\alpha\beta+\lambda+\frac{\varepsilon\gamma}{1-f(\rho_1,\delta)}} q_{0,0,0}.$$

If there are no infectious hosts present in the population (i.e. $i = j = k = 0$), then a local outbreak will not occur and so $q_{0,0,0} = 1$. Assuming that transmission chains arising from two infectious individuals are independent gives $q_{1,0,1} = q_{1,0,0}\, q_{0,0,1}$ and $q_{2,0,0} = q_{1,0,0}^2$. Hence,

$$q_{1,0,0} = a\xi q_{1,0,0}\, q_{0,0,1} + a(1-\xi)q_{1,0,0}^2 + bq_{0,1,0} + (1-a-b), \quad (3)$$

where $a = \frac{\alpha\beta}{\alpha\beta+\lambda+\frac{\varepsilon\gamma}{1-f(\rho_{1,\delta})}}$, $b = \frac{\lambda}{\alpha\beta+\lambda+\frac{\varepsilon\gamma}{1-f(\rho_1,\delta)}}$.

Similarly, considering the probability of a local outbreak failing to occur starting from a single symptomatic host gives

$$q_{0,1,0} = \frac{\xi\beta}{\beta+\frac{\gamma}{1-f(\rho_{2,}\delta)}+\mu} q_{0,1,1} + \frac{(1-\xi)\beta}{\beta+\frac{\gamma}{1-f(\rho_{2,}\delta)}+\mu} q_{1,1,0} + \frac{\frac{\gamma}{1-f(\rho_{2,}\delta)}+\mu}{\beta+\frac{\gamma}{1-f(\rho_{2,}\delta)}+\mu} q_{0,0,0}.$$

As before, noting that $q_{0,0,0} = 1$ and assuming that different infection lineages are independent leads to

$$q_{0,1,0} = c\xi q_{01,0} q_{0,0,1} + c(1-\xi) q_{1,0,0} q_{0,1,0} + (1-c), \qquad (4)$$

where $c = \frac{\beta}{\beta+\frac{\gamma}{1-f(\rho_{2,}\delta)}+\mu}$.

Finally, considering the probability of a local outbreak failing to occur starting from a single asymptomatic host gives

$$q_{0,0,1} = d\xi q_{0,0,1}^2 + d(1-\xi) q_{1,0,0} q_{0,0,1} + (1-d), \qquad (5)$$

where $d = \frac{\eta\beta}{\eta\beta+\nu+\frac{\epsilon\gamma}{1-f(\rho_{1,}\delta)}}$.

Equations (3), (4) and (5) may be combined to give a single quartic equation for $q_{0,0,1}$, yielding four sets of solutions for $q_{1,0,0}, q_{0,1,0}$ and $q_{0,0,1}$ (see Supplementary Text S1). It is straightforward to verify that $q_{1,0,0} = q_{0,1,0} = q_{0,0,1} = 1$ is always a solution, and further solutions can be found numerically. The appropriate solution to take is the minimal non-negative real solution $q_{1,0,0} = q^*_{1,0,0},\ q_{0,1,0} = q^*_{0,1,0},\ q_{0,0,1} = q^*_{0,0,1}$ (see Supplementary Text S1). Then, the probability of a local outbreak occurring beginning from a single presymptomatic host is given by

$$p_{1,0,0} = 1 - q^*_{1,0,0},$$

with equivalent expressions holding for $p_{0,1,0}$ and $p_{0,0,1}$ (the probability of a local outbreak occurring beginning from a single symptomatic host or a single asymptomatic host, respectively).

Throughout, we consider the probability p of a local outbreak starting from a single nonsymptomatic host entering the population, accounting for the possibility that the nonsymptomatic host is either presymptomatic or asymptomatic:

$$p = (1 - \xi)p_{1,0,0} + \xi p_{0,0,1}.$$

3. Results

3.1 Probability of a local outbreak

We considered the effect of R_0 and the duration of the presymptomatic and asymptomatic periods on the probability of a local outbreak when a nonsymptomatic host enters a new host population (Fig 2). We examined presymptomatic periods of length $1/\lambda = 1$ day, $1/\lambda = 2$ days and $1/\lambda = 4$ days; in each case, the duration of the asymptomatic period ($1/\nu$ days) was adjusted so that the relative proportion of infections arising from asymptomatic hosts compared to presymptomatic hosts remained fixed ($K_a/K_p = 0.218$, as in the baseline case). If instead nonsymptomatic infections are not accounted for, the infectious period follows an exponential distribution and the probability of a local outbreak is given by $p = 1 - 1/R_0$ (red dash-dotted line in Fig 2A). Including nonsymptomatic infection in the model therefore led to an increased risk of a local outbreak in the absence of surveillance intensification (Fig 2A).

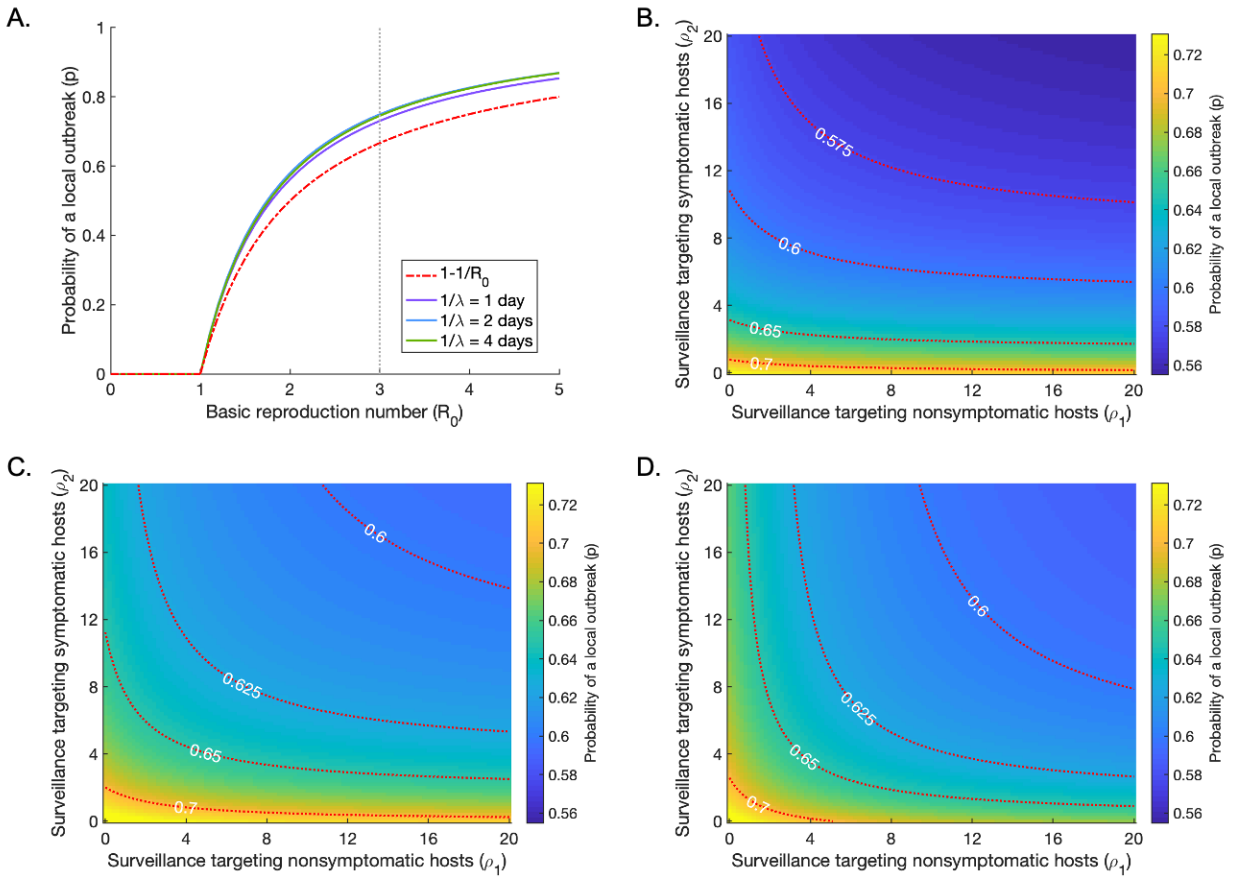

Fig 2. The effect of the duration of the presymptomatic and asymptomatic periods on the probability of a local outbreak (p), starting from a single nonsymptomatic host. A. The probability of a local outbreak as a function of the basic reproduction number R_0, for presymptomatic periods of lengths $1/\lambda = 1$ day (purple), $1/\lambda = 2$ days (blue) and $1/\lambda = 4$ days (green) in the absence of enhanced surveillance ($\rho_1 = \rho_2 = 0$). In each case, the duration of the asymptomatic period ($1/\nu$) is adjusted so that the relative proportion of infections arising from asymptomatic hosts compared to presymptomatic hosts remains constant ($K_a/K_p = 0.218$, as in the baseline case). The red dash-dotted line indicates the probability of a local outbreak in the absence of nonsymptomatic transmission. The vertical grey dotted line indicates $R_0 = 3$, the baseline value used throughout. B. The probability of a local outbreak as a function of the surveillance intensification efforts ρ_1 and ρ_2, for $1/\lambda = 1$ day. C. The analogous figure to B but with $1/\lambda = 2$ days. D. The analogous figure to B but with $1/\lambda = 4$ days. Red dotted lines indicate contours of constant local outbreak probability (i.e. lines on which the probability of a local outbreak takes the values shown). The

298 value of β is varied in each panel to fix $R_0 = 3$. All other parameter values are held fixed at the values in
299 Table 1 (except where stated).
300
301 We then considered the dependence of the probability of a local outbreak on the intensity of
302 surveillance targeting nonsymptomatic and symptomatic hosts (Fig 2B-D). The maximum value of
303 the surveillance intensification effort that we considered (given by ρ_1 or ρ_2 values of 20)
304 corresponded to a 76% reduction in the expected time to isolation (blue line in Fig 1B), i.e. a 76%
305 reduction in $\frac{1}{\varepsilon\gamma}$ or $\frac{1}{\gamma}$.
306
307 The length of the presymptomatic and asymptomatic periods significantly affected the dependence
308 of the probability of a local outbreak on the level of surveillance targeted at nonsymptomatic and
309 symptomatic hosts. In Fig 2B, in which the duration of the presymptomatic period was 1 day,
310 increasing surveillance targeted at nonsymptomatic hosts (ρ_1) had a limited effect on the
311 probability of a local outbreak, while increasing surveillance targeted at symptomatic hosts (ρ_2)
312 had a more significant effect. For example, increasing the surveillance effort targeted at
313 nonsymptomatic hosts to $\rho_1 = 5$ (a 67% reduction in the time to isolation) only reduced the
314 probability of a local outbreak from 0.730 to 0.716, whereas the equivalent effort targeted at
315 symptomatic hosts ($\rho_2 = 5$) reduced the probability to 0.630. As shown in Figs 3C and D,
316 however, when the presymptomatic and asymptomatic periods were longer, the benefit of directing
317 surveillance resources towards detecting nonsymptomatic individuals increased. This was because
318 longer presymptomatic and asymptomatic periods increased the proportion of infections generated
319 by nonsymptomatic individuals ($K_p + K_a$, see equations (1) and (2)); a presymptomatic period of 1
320 day, 2 days and 4 days corresponded to values of $K_p + K_a$ equal to 0.424, 0.595 and 0.746,
321 respectively.

3.2 Optimising surveillance enhancement

We next considered in more detail the impact of surveillance targeted at nonsymptomatic hosts (ρ_1) relative to the impact of surveillance targeted at symptomatic hosts (ρ_2). For our baseline parameter values, we considered the probability of a local outbreak starting from a single imported nonsymptomatic individual for a range of values of ρ_1 and ρ_2. We calculated the steepest descent contours (white lines in Fig 3A) numerically using a gradient maximisation approach, in which at each point the contour direction was determined by minimising the local outbreak probability over a fixed search radius (see Supplementary Text S2 and Supplementary Fig S2). These contours indicate how ρ_1 and ρ_2 should be altered to maximise the reduction in the probability of a local outbreak. In this case, enhancing surveillance targeting both symptomatic and nonsymptomatic hosts is always optimal (the steepest descent contours are neither horizontal nor vertical).

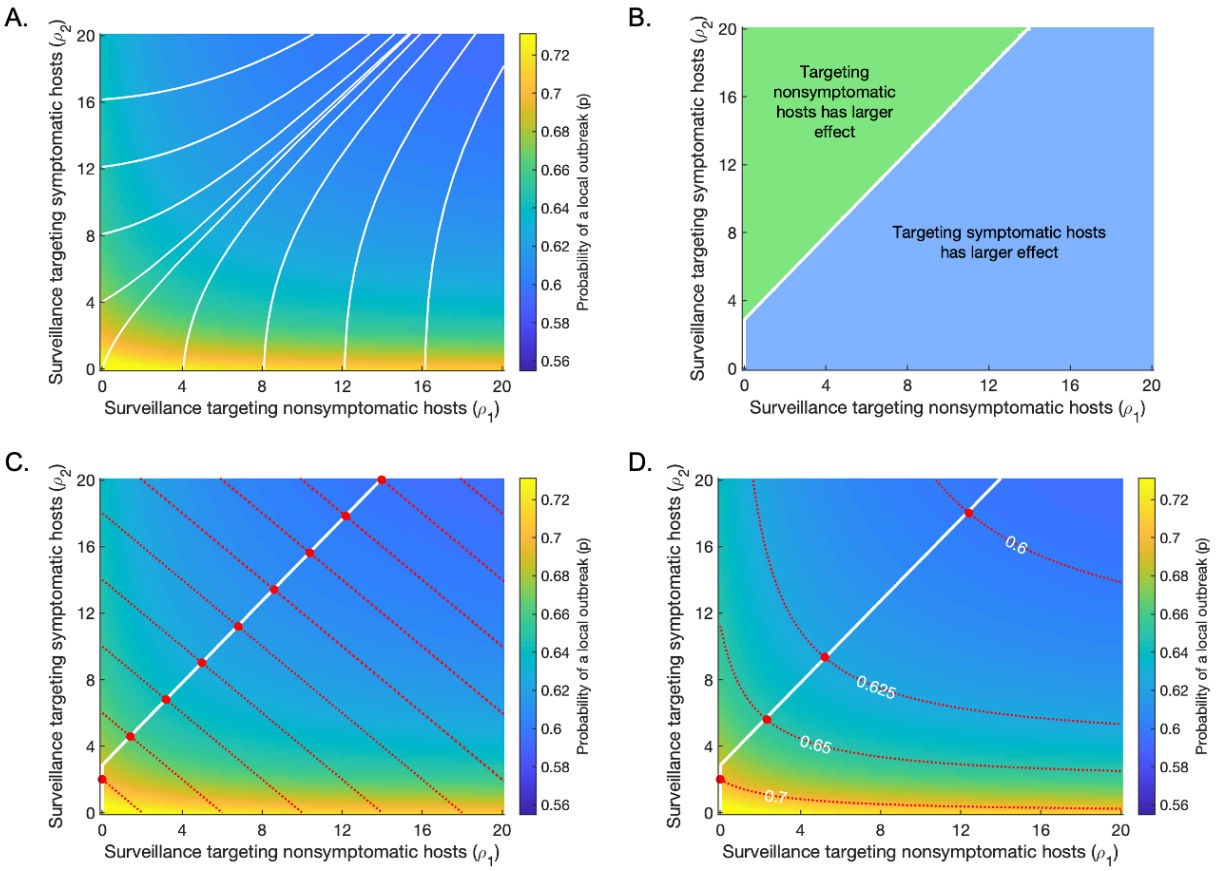

Fig 3. Optimal surveillance strategies to reduce the probability of a local outbreak (p) starting from a single nonsymptomatic host. A. The local outbreak probability for different values of ρ_1 and ρ_2, with the steepest descent contours overlaid (white lines). For the maximum reduction in the probability of a local outbreak at each point, surveillance must be enhanced for both nonsymptomatic and symptomatic individuals, with different levels of prioritisation depending on the current values of ρ_1 and ρ_2. B. Values of ρ_1 and ρ_2 for which increasing surveillance for nonsymptomatic hosts (i.e. increasing ρ_1) is more effective at reducing the local outbreak probability than increasing surveillance for symptomatic hosts (i.e. increasing ρ_2) (green region) and vice versa (blue region). The white line represents the steepest descent contour starting from $\rho_1 = \rho_2 = 0$, under the constraint that surveillance can only be enhanced for either symptomatic or nonsymptomatic hosts at any time. The diagonal section of the steepest descent contour is made up of small horizontal and vertical sections. C. Strategies for minimising the local outbreak probability for a given fixed total surveillance effort ($\rho_1 + \rho_2 = C$). Red dotted lines indicate contours on which $\rho_1 + \rho_2$ is constant (i.e. lines on which $\rho_1 + \rho_2$ takes the values shown); red circles indicate the points along these

contours at which the local outbreak probability is minimised. The white line indicates the optimal surveillance enhancement strategy if the maximum possible surveillance level (i.e. the maximum value of $\rho_1 + \rho_2 = C$) is increased. D. Strategies for minimising the surveillance effort required to achieve a pre-specific risk level (an "acceptable" local outbreak probability). Red dotted lines indicate contours of constant local outbreak probability (i.e. lines on which the probability of a local outbreak takes the values shown); red circles indicate the points along these contours at which the total surveillance effort $\rho_1 + \rho_2$ is minimised. The white line indicates the optimal strategy to follow if the pre-specified risk level is increased or reduced.

We then considered a scenario in which, at any time, it is only possible to direct resources towards enhancing surveillance of either nonsymptomatic individuals or symptomatic individuals (e.g. antigen testing of nonsymptomatic contacts of known infectious individuals, or screening for symptomatic individuals at public events). In Fig 3B, the blue region represents values of ρ_1 and ρ_2 for which enhancing surveillance targeting symptomatic hosts (i.e. increasing ρ_2) leads to a larger reduction in the local outbreak probability than enhancing surveillance targeting nonsymptomatic hosts (i.e. increasing ρ_1). In contrast, in the green region, enhancing surveillance of nonsymptomatic individuals is more effective than enhancing surveillance of symptomatic individuals. The white line represents the steepest descent contour starting from $\rho_1 = \rho_2 = 0$, under the constraint that surveillance can only be enhanced for symptomatic or nonsymptomatic hosts at any time.

Practical deployment of surveillance is often subject to logistical constraints, and policy-makers may wish to design surveillance strategies to achieve a specific objective – for example, to maximise the effectiveness of limited resources or to minimise the cost of achieving a desired outcome. We therefore also considered the following two examples of such objectives.

Objective 1: Minimise the probability of a local outbreak for a fixed total surveillance effort. First, we considered the question: given a fixed maximum surveillance effort ($\rho_1 + \rho_2 = C$), how should surveillance be targeted at nonsymptomatic and symptomatic hosts? This involves setting the values of ρ_1 and ρ_2 to minimise the local outbreak probability. The optimal strategies in this case are shown in Fig 3C. The red dotted lines represent contours along which the total surveillance effort $\rho_1 + \rho_2$ is held constant (i.e. different values of C). On each contour, the red circle indicates the point at which the local outbreak probability is minimised.

If surveillance resources are increased (i.e. C increases), a further question is how surveillance should then be increased. In Fig 3C, the white line represents the contour of steepest descent, under the constraint that the total change in surveillance effort ($\rho_1 + \rho_2$) is held constant at each step (rather than a constant search radius, as in Fig 3A – for more details, see Supplementary Text S2 and Supplementary Fig S2). This contour coincides exactly with that shown in Fig 3B.

These results indicate that, if surveillance resources are such that C is greater than 2.8 (corresponding to a 59% reduction in time to isolation of symptomatic hosts), the optimal surveillance strategy involves both enhanced surveillance of symptomatic individuals and nonsymptomatic individuals (the red dots correspond to strictly positive values of both ρ_1 and ρ_2, unless C is less than 2.8).

Objective 2: Minimise the total surveillance effort to achieve a pre-specified reduction in the probability of a local outbreak. Second, we considered the question: given a pre-specified acceptable risk level (i.e. probability of a local outbreak), how should the surveillance level

targeted at nonsymptomatic and symptomatic hosts be chosen? This involves choosing ρ_1 and ρ_2 to minimise $\rho_1 + \rho_2$ along a given contour corresponding to a fixed local outbreak probability (red dotted lines in Fig 3D). On each contour, the red circle indicates the point along that contour at which the total surveillance effort $\rho_1 + \rho_2$ is minimised. These optimal points also lie exactly along the line on which enhancing surveillance targeted at symptomatic hosts is equally effective compared to enhancing surveillance targeted at nonsymptomatic hosts.

As long as the target local outbreak probability is less than 0.69, optimal surveillance involves enhanced surveillance of nonsymptomatic individuals as well as symptomatic individuals. For example, in order to reduce the local outbreak probability to 0.6, the optimal approach is to deploy resources such that $\rho_1 = 12.4$ (a 74% reduction in time to isolation of nonsymptomatic individuals) and $\rho_2 = 18.0$ (a 76% reduction in time to isolation of symptomatic individuals).

Plots analogous to Fig 3D in which the parameters were varied from their baseline values are shown in Supplementary Figs S3-12. In each case that we considered, our main finding was unchanged. There always exists a threshold local outbreak probability such that, if the target local outbreak probability is below this threshold, the optimal strategy for further reduction in the local outbreak probability involves enhancing surveillance targeting both nonsymptomatic and symptomatic individuals.

4. Discussion

A key component of infectious disease epidemic management is inferring the risk of outbreaks in different locations [5-8, 11, 41, 42]. Surveillance and control strategies can be introduced to reduce the risk that imported cases will lead to local outbreaks [12, 13, 43-46]. However, for a range of

422 pathogens, public health measures are hindered by nonsymptomatic infectious hosts who can
423 transmit the pathogen yet are challenging to detect [16, 42, 44, 47-49].
424
425 Here, we showed how the probability of a local outbreak can be estimated using a branching
426 process model that accounts for transmission from nonsymptomatic infected individuals (Fig 1).
427 The model can be used to assess the local outbreak probability for different surveillance strategies
428 that target nonsymptomatic or symptomatic hosts (Fig 2). Previous studies have shown that
429 detection of nonsymptomatic infections can be a key component of epidemic forecasting [42] and
430 containment [44], and have demonstrated the benefits of identifying and isolating infectious
431 nonsymptomatic hosts to reduce transmission [16, 17]. We focused instead on investigating how
432 surveillance should be targeted at nonsymptomatic or symptomatic hosts in order to reduce the
433 probability that cases imported to new locations will trigger a local outbreak (Fig 3A,B). We also
434 showed how the optimal surveillance level targeting these two groups can be assessed when
435 surveillance resources are limited and policy-makers have specific objectives (Fig 3C,D). In each
436 case, our main conclusion was that surveillance for nonsymptomatic infected hosts ($\rho_1 > 0$) can
437 be an important component of reducing the local outbreak risk during epidemics. This result has
438 broad implications, and our analysis could be extended to assess the potential for containing
439 outbreaks at their source using a range of specific interventions targeting symptomatic and
440 nonsymptomatic hosts.
441
442 Our goal here was to use the simplest possible model to explore the effects of surveillance of
443 nonsymptomatic and symptomatic individuals on the risk of local outbreaks. However, this model
444 is not without its limitations. One area of uncertainty is the precise values of the parameters
445 governing pathogen transmission and control. In this article, we chose a baseline set of parameter

446 values that is consistent with the findings of studies conducted during the COVID-19 pandemic,
447 although constructing a detailed transmission model for this pandemic was not our main focus. For
448 example, we set the relative rates at which presymptomatic and asymptomatic individuals generate
449 new infections compared to symptomatic individuals so that 48.9% of transmissions arise from
450 presymptomatic infectors, and 10.6% arise from asymptomatic infectors [16]. While this is in line
451 with reported estimates [50, 51], there is substantial variation between studies. Similarly, the
452 proportion of individuals who experience a fully asymptomatic course of infection (denoted by ξ
453 in our model) is subject to a considerable degree of uncertainty. Here, we chose $\xi = 0.2$ as the
454 baseline value [32-34] but estimates in the literature range from 0.04 to over 0.8 [33, 52-54]. We
455 therefore also conducted sensitivity analyses in which we explored a range of different values of
456 model parameters (Supplementary Text S3 and Supplementary Figs S3-12). In each case that we
457 considered, our main conclusion was unchanged: surveillance of nonsymptomatic individuals can
458 contribute to reducing the risk of local outbreaks. This result is expected to hold for epidemics of
459 any pathogen for which nonsymptomatic individuals contribute significantly to transmission.
460
461 For our modelling approach to be used to make precise quantitative predictions during epidemics,
462 it would be necessary to update the model to include the range of different specific surveillance
463 and control interventions that are in place. For example, detection of nonsymptomatic infected
464 individuals is facilitated by contact tracing and antigen testing, which are carried out routinely
465 during epidemics and can be included in models explicitly [12, 44, 55, 56]. Reductions in contacts
466 due to social distancing strategies and school or workplace closures could also be accounted for
467 [57, 58], although such interventions are often introduced after a local outbreak has begun rather
468 than in the initial phase of a potential local outbreak as considered here. We modelled the level of
469 surveillance targeted at nonsymptomatic and symptomatic hosts in a simple way, using a function

describing the relationship between surveillance effort and effectiveness (Fig 1B). We assumed that this general functional relationship could be applied to interventions targeting both symptomatic and nonsymptomatic hosts, accounting for logistical differences in the ease of targeting either group by scaling the effectiveness of surveillance for nonsymptomatic hosts using the parameter ε (results are shown for different values of ε in Supplementary Fig S8). In principle, it would be possible to include entirely different functional forms describing the relationship between surveillance effort and effectiveness for strategies targeting symptomatic and nonsymptomatic individuals, and these could be tailored to the effects of particular interventions. If different public health measures are included in the model explicitly, then it would be possible to increase the accuracy of assessments of the relative public health benefits of specific interventions that only target symptomatic individuals (e.g. screening for passengers with heightened temperatures at airports [59, 60]) compared to interventions that also target nonsymptomatic hosts (e.g. travel bans or quarantine of all inbound passengers [61, 62]). Of course, this would require data from which the relative effectiveness of different measures could be inferred.

The underlying transmission model could also be extended to include additional realism in several ways. Transmission dynamics are influenced by marked heterogeneities in the patterns of contacts between individuals in different age groups [63, 64], and, for COVID-19, susceptibility to infection, the likelihood of developing symptoms, and the average severity of those symptoms increase with age [65, 66]. Age-dependent variation in the proportion of asymptomatic cases in particular implies that the optimal balance of surveillance between symptomatic and nonsymptomatic hosts may differ between age groups. An age-structured version of the model presented here is a focus of our ongoing research. Similarly, for a range of infectious diseases, the

494 distribution characterising the number of secondary infections generated by each infected host (the
495 offspring distribution) exhibits a high degree of overdispersion [67-70]. For a fixed value of R_0, a
496 higher degree of overdispersion increases the likelihood that initial cases will fade out without
497 leading to a local outbreak [71, 72], and suggests that greater reductions in local outbreak risks
498 could theoretically be achieved for the same surveillance effort, if potential superspreaders or
499 superspreading events can be identified and targeted.
500
501 Despite the necessary simplifications, we have shown how the risk of local outbreaks can be
502 estimated during epidemics using a branching process model that includes nonsymptomatic
503 infectious hosts explicitly. Determining the extent to which nonsymptomatic individuals contribute
504 to transmission is essential early in emerging epidemics of a novel pathogen. As we have shown, if
505 transmissions occur from nonsymptomatic infectors, dedicating surveillance resources towards
506 finding nonsymptomatic cases can be an important component of public health measures that aim
507 to prevent local outbreaks.
508

509 ## Acknowledgements

510 Thank you to Andrew Wood and Charles Tolkien-Gillett for proofreading.
511

512 ## Funding

513 FALR acknowledges funding from the Biotechnology and Biological Sciences Research Council
514 (UKRI-BBSRC), grant number BB/M011224/1. SF and RNT acknowledge funding from the
515 Wellcome Trust, grant number 210758/Z/18/Z. RNT also acknowledges funding from Christ
516 Church (University of Oxford) via a Junior Research Fellowship. CAD acknowledges funding
517 from the MRC Centre for Global Infectious Disease Analysis (reference MR/R015600/1), jointly

518 funded by the UK Medical Research Council (MRC) and the UK Foreign, Commonwealth &
519 Development Office (FCDO) under the MRC/FCDO Concordat agreement, and is also part of the
520 EDCTP2 programme supported by the European Union.

521

522 References

523 [1] Bloom, D.E. & Cadarette, D. 2019 Infectious Disease Threats in the Twenty-First Century:
524 Strengthening the Global Response. *Front. Immunol.* **10**. (doi:10.3389/fimmu.2019.00549).
525 [2] Morens, D.M. & Fauci, A.S. 2013 Emerging Infectious Diseases: Threats to Human Health
526 and Global Stability. *Public Library of Science: Pathogens* **9**, e1003467.
527 (doi:10.1371/journal.ppat.1003467).
528 [3] Sigfrid, L., Maskell, K., Bannister, P.G., Ismail, S.A., Collinson, S., Regmi, S., Blackmore, C.,
529 Harriss, E., Longuere, K.-S., Gobat, N., et al. 2020 Addressing challenges for clinical research
530 responses to emerging epidemics and pandemics: a scoping review. *BMC Med.* **18**, 190-190.
531 (doi:10.1186/s12916-020-01624-8).
532 [4] Thompson, R.N. & Brooks-Pollock, E. 2019 Detection, forecasting and control of infectious
533 disease epidemics: modelling outbreaks in humans, animals and plants. *Philos. Trans. R. Soc.*
534 *Lond., B, Biol. Sci.* **374**, 20190038-20190038. (doi:10.1098/rstb.2019.0038).
535 [5] Althaus, C.L., Low, N., Musa, E.O., Shuaib, F. & Gsteiger, S. 2015 Ebola virus disease
536 outbreak in Nigeria: Transmission dynamics and rapid control. *Epidemics* **11**, 80-84.
537 (doi:10.1016/j.epidem.2015.03.001).
538 [6] Boldog, P., Tekeli, T., Vizi, Z., Denes, A., Bartha, F.A. & Rost, G. 2020 Risk Assessment of
539 Novel Coronavirus COVID-19 Outbreaks Outside China. *J. Clin. Med.* **9**, 571.
540 (doi:doi.org/10.3390/jcm9020571).

[7] Daon, Y., Thompson, R.N. & Obolski, U. 2020 Estimating COVID-19 outbreak risk through air travel. *J. Travel Med.* **27**. (doi:10.1093/jtm/taaa093).

[8] Lashari, A.A. & Trapman, P. 2018 Branching process approach for epidemics in dynamic partnership network. *J. Math. Biol.* **76**, 265-294. (doi:10.1007/s00285-017-1147-0).

[9] Nishiura, H., Cook, A.R. & Cowling, B.J. 2011 Assortativity and the Probability of Epidemic Extinction: A Case Study of Pandemic Influenza A (H1N1-2009). *Interdiscip. Perspect. Infect. Dis.* **2011**, 194507-194507. (doi:10.1155/2011/194507).

[10] Thompson, R.N., Jalava, K. & Obolski, U. 2019 Sustained transmission of Ebola in new locations: more likely than previously thought. *The Lancet Infectious Diseases* **19**, 1058-1059. (doi:10.1016/S1473-3099(19)30483-9).

[11] Thompson, R.N., Thompson, C.P., Pelerman, O., Gupta, S. & Obolski, U. 2019 Increased frequency of travel in the presence of cross-immunity may act to decrease the chance of a global pandemic. *Philos. Trans. R. Soc. Lond., B, Biol. Sci.* **374**, 20180274. (doi:10.1098/rstb.2018.0274).

[12] Hellewell, J., Abbott, S., Gimma, A., Bosse, N.I., Jarvis, C.I., Russell, T.W., Munday, J.D., Kucharski, A.J., Edmunds, W.J., Sun, F., et al. 2020 Feasibility of controlling COVID-19 outbreaks by isolation of cases and contacts. *The Lancet Global Health* **8**, e488-e496. (doi:10.1016/S2214-109X(20)30074-7).

[13] Thompson, R.N. 2020 Novel Coronavirus Outbreak in Wuhan, China, 2020: Intense Surveillance Is Vital for Preventing Sustained Transmission in New Locations. *Journal of Clinical Medicine* **9**, 498. (doi:10.3390/jcm9020498).

[14] Lauer, S.A., Grantz, K.H., Bi, Q., Jones, F.K., Zheng, Q., Meredith, H.R., Azman, A.S., Reich, N.G. & Lessler, J. 2020 The Incubation Period of Coronavirus Disease 2019 (COVID-19) From Publicly Reported Confirmed Cases: Estimation and Application. *Ann. Intern. Med.* **172**, 577-582. (doi:10.7326/M20-0504).

565 [15] McAloon, C., Collins, A., Hunt, K., Barber, A., Byrne, A.W., Butler, F., Casey, M., Griffin,
566 J., Lane, E., McEvoy, D., et al. 2020 Incubation period of COVID-19: a rapid systematic review
567 and meta-analysis of observational research. *BMJ Open* **10**, e039652. (doi:10.1136/bmjopen-2020-
568 039652).
569 [16] Ferretti, L., Wymant, C., Kendall, M., Zhao, L., Nurtay, A., Abeler-Dorner, L., Parker, M.,
570 Bonsall, D. & Fraser, C. 2020 Quantifying SARS-CoV-2 transmission suggests epidemic control
571 with digital contact tracing. *Science* **368**, eabb6936. (doi:10.1126/science.abb6936).
572 [17] Moghadas, S.M., Fitzpatrick, M.C., Sah, P., Pandey, A., Shoukat, A., Singer, B.H. & Galvani,
573 A. 2020 The implications of silent transmission for the control of COVID-19 outbreaks. *Proc.*
574 *Natl. Acad. Sci. U. S. A.* **117**, 17513-17515. (doi:10.1073/pnas.2008373117).
575 [18] Tindale, L.C., Stockdale, J.E., Coombe, M., Garlock, E.S., Lau, W.Y.V., Saraswat, M.,
576 Zhang, L., Chen, D., Wallinga, J. & Colijn, C. 2020 Evidence for transmission of COVID-19 prior
577 to symptom onset. *eLife* **9**, e57149. (doi:10.7554/eLife.57149).
578 [19] Tong, Z.-D., Tang, A., Li, K.-F., Li, P., Wang, H.-L., Yi, J.-P., Zhang, Y.-L. & Yan, J.-B.
579 2020 Potential Presymptomatic Transmission of SARS-CoV-2, Zhejiang Province, China, 2020.
580 *Emerging Infectious Diseases* **26**, 1052-1054. (doi:10.3201/eid2605.200198).
581 [20] Wei, W.E., Li, Z., Chiew, C.J., Yong, S.E., Toh, M.P. & Lee, V.J. 2020 Presymptomatic
582 Transmission of SARS-CoV-2 — Singapore, January 23–March 16, 2020. *Morbidity and*
583 *Mortality Weekly Report* **69**, 411-415. (doi:10.15585/mmwr.mm6914e1external icon).
584 [21] Bai, Y., Yao, L., Wei, T., Tian, F., Jin, D.-Y., Chen, L. & Wang, M. 2020 Presumed
585 Asymptomatic Carrier Transmission of COVID-19. *J. Am. Med. Assoc.* **323**, 1406-1407.
586 (doi:10.1001/jama.2020.2565).

587 [22] Furukawa, N.W., Brooks, J.T. & Sobel, J. 2020 Evidence Supporting Transmission of Severe
588 Acute Respiratory Syndrome Coronavirus 2 While Presymptomatic or Asymptomatic. *Emerging*
589 *Infectious Diseases* **26**, e201595. (doi:10.3201/eid2607.201595).
590 [23] Anderson, D. & Watson, R. 1980 On the spread of a disease with gamma distributed latent
591 and infectious periods. *Biometrika* **67**, 191-198. (doi:10.1093/biomet/67.1.191).
592 [24] Bartlett, M.S. 1964 The Relevance of Stochastic Models for Large-Scale Epidemiological
593 Phenomena. *J. Roy. Stat. Soc. Ser. C. (Appl. Stat.)* **13**, 2-8. (doi:10.2307/2985217).
594 [25] Craft, M.E., Beyer, H.L. & Haydon, D.T. 2013 Estimating the Probability of a Major
595 Outbreak from the Timing of Early Cases: An Indeterminate Problem? *PLoS One* **8**, e57878-
596 e57878. (doi:10.1371/journal.pone.0057878).
597 [26] Lloyd, A.L., Zhang, J. & Root, A.M. 2007 Stochasticity and heterogeneity in host-vector
598 models. *J. R. Soc. Interface* **4**, 851-863. (doi:10.1098/rsif.2007.1064).
599 [27] Matthews, L., Haydon, D.T., Shaw, D.J., Chase-Topping, M.E., Keeling, M.J. & Woolhouse,
600 M.E.J. 2003 Neighbourhood control policies and the spread of infectious diseases. *Proceedings of*
601 *the Royal Society B: Biological Sciences* **270**, 1659-1666. (doi:10.1098/rspb.2003.2429).
602 [28] Lai, C.-C., Shih, T.-P., Ko, W.-C., Tang, H.-J. & Hsueh, P.-R. 2020 Severe acute respiratory
603 syndrome coronavirus 2 (SARS-CoV-2) and coronavirus disease-2019 (COVID-19): The
604 epidemic and the challenges. *International Journal of Antimicrobial Agents* **55**, 105924.
605 (doi:10.1016/j.ijantimicag.2020.105924).
606 [29] Liu, Y., Gayle, A.A., Wilder-Smith, A. & Rocklov, J. 2020 The reproductive number of
607 COVID-19 is higher compared to SARS coronavirus. *Journal of Travel Medicine* **27**, taaa021.
608 (doi:10.1093/jtm/taaa021).

609 [30] Zhai, P., Ding, Y., Wu, X., Long, J., Zhong, Y. & Li, Y. 2020 The epidemiology, diagnosis
610 and treatment of COVID-19. *International Journal of Antimicrobial Agents* **55**, 105955-105955.
611 (doi:10.1016/j.ijantimicag.2020.105955).
612 [31] Zhao, S., Lin, Q., Ran, J., Musa, S.S., Yang, G., Wang, W., Lou, Y., Gao, D., Yang, L., He,
613 D., et al. 2020 Preliminary estimation of the basic reproduction number of novel coronavirus
614 (2019-nCoV) in China, from 2019 to 2020: A data-driven analysis in the early phase of the
615 outbreak. *International Journal of Infectious Diseases* **92**, 214-217.
616 (doi:10.1016/j.ijid.2020.01.050).
617 [32] Buitrago-Garcia, D., Egli-Gany, D., Counotte, M.J., Hossman, S., Imeri, H., Ipekci, A.M.,
618 Salanti, G. & Low, N. 2020 Occurrence and transmission potential of asymptomatic and
619 presymptomatic SARS-CoV-2 infections: A living systematic review and meta-analysis. *PLoS*
620 *Med.* **17**, e1003346. (doi:10.1371/journal.pmed.1003346).
621 [33] Byambasuren, O., Cardona, M., Bell, K., Clark, J., McLaws, M.-L. & Glasziou, P. 2020
622 Estimating the extend of asymptomatic COVID-19 and its potential for community transmission:
623 Systematic review and meta-analysis. *JAMMI* **5**, 223-234. (doi:10.3138/jammi-2020-0030).
624 [34] He, J., Guo, Y., Mao, R. & Zhang, J. 2020 Proportion of asymptomatic coronavirus disease
625 2019: A systematic review and meta-analysis. *J. Med. Virol.* **93**, 820-830.
626 (doi:10.1002/jmv.26326).
627 [35] Li, Q., Guan, X., Wu, P., Wang, X., Zhou, L., Tong, Y., Ren, R., Leung, K.S.M., Lau,
628 E.H.Y., Wong, J.Y., et al. 2020 Early Transmission Dynamics in Wuhan, China, of Novel
629 Coronavirus–Infected Pneumonia. *N. Engl. J. Med.* **382**, 1199-1207.
630 (doi:10.1056/NEJMoa2001316).
631 [36] Arons, M.M., Hatfield, K.M., Reddy, S.C., Kimball, A., James, A., Jacobs, J.R., Taylor, J.,
632 Spicer, K., Bardossy, A.C., Oakley, L.P., et al. 2020 Presymptomatic SARS-CoV-2 Infections and

633 Transmission in a Skilled Nursing Facility. *The New England Journal of Medicine* **382**, 2081-
634 2090. (doi:10.1056/NEJMoa2008457).
635 [37] Bullard, J., Dust, K., Funk, D., Strong, J.E., Alexander, D., Garnett, L., Boodman, C., Bello,
636 A., Hedley, A., Schiffman, Z., et al. 2020 Predicting Infectious Severe Acute Respiratory
637 Syndrome Coronavirus 2 From Diagnostic Samples. *Clinical Infectious Diseases*, ciaa638.
638 (doi:10.1093/cid/ciaa638).
639 [38] Wolfel, R., Corman, V.M., Guggemos, W., Seilmaier, M., Zange, S., Muller, M.A.,
640 Niemeyer, D., Jones, T.C., Vollmar, P., Rothe, C., et al. 2020 Virological assessment of
641 hospitalized patients with COVID-2019. *Nature* **581**, 465-469. (doi:10.1038/s41586-020-2196-x).
642 [39] Nasell, I. 1995 The Threshold Concept in Stochastic Epidemic and Endemic Models. In
643 *Epidemic Models: Their Structure and Relation to Data* (ed. D. Mollison), pp. 71-83. Cambridge,
644 UK, Cambridge University Press.
645 [40] Britton, T. 2010 Stochastic epidemic models: A survey. *Math. Biosci.* **225**, 24-35.
646 (doi:10.1016/j.mbs.2010.01.006).
647 [41] Thompson, R.N., Gilligan, C.A. & Cunniffe, N.J. 2020 Will an outbreak exceed available
648 resources for control? Estimating the risk from invading pathogens using practical definitions of a
649 severe epidemic. *J. R. Soc. Interface* **17**. (doi:10.1098/rsif.2020.0690).
650 [42] Thompson, R.N., Gilligan, C.A. & Cunniffe, N.J. 2016 Detecting Presymptomatic Infection
651 Is Necessary to Forecast Major Epidemics in the Earliest Stages of Infectious Disease Outbreaks.
652 *PLoS Comput. Biol.* **12**, e1004836. (doi:10.1371/journal.pcbi.1004836).
653 [43] Charleston, B., Bankowski, B.M., Gubbins, S., Chase-Topping, M.E., Schley, D., Howey, R.,
654 Barnett, P.V., Gibson, D., Juleff, N.D. & Woolhouse, M.E.J. 2011 Relationship Between Clinical
655 Signs and Transmission of an Infectious Disease and the Implications for Control. *Science* **332**,
656 726-729. (doi:10.1126/science.1199884).

[44] Fraser, C., Riley, S., Anderson, R.M. & Ferguson, N.M. 2004 Factors that make an infectious disease outbreak controllable. *Proc. Natl. Acad. Sci. U. S. A.* **101**, 6146-6151. (doi:10.1073/pnas.0307506101).

[45] Martinez, L. 2000 Global infectious disease surveillance. *Int. J. Infect. Dis.* **4**, 222-228. (doi:10.1016/s1201-9712(00)90114-0).

[46] Milinovich, G.J., Williams, G.M., Clements, A.C.A. & Hu, W. 2014 Internet-based surveillance systems for monitoring emerging infectious diseases. *The Lancet Infectious Diseases* **14**, 160-168. (doi:10.1016/S1473-3099(13)70244-5).

[47] Gu, Y., Komiya, N., Kamiya, H., Yasui, Y., Taniguchi, K. & Okabe, N. 2011 Pandemic (H1N1) 2009 Transmission during Presymptomatic Phase, Japan. *Emerging Infectious Diseases* **17**, 1737-1739. (doi:10.3201/eid1709.101411).

[48] Ip, D.K.M., Lau, L.L.H., Leung, N.H.L., Fang, V.J., Chan, K.-H., Chu, D.K.W., Leung, G.M., Peiris, J.S.M., Uyeki, T.M. & Cowling, B.J. 2016 Viral Shedding and Transmission Potential of Asymptomatic and Paucisymptomatic Influenza Virus Infections in the Community. *Clin. Infect. Dis.* **64**, 736-742. (doi:10.1093/cid/ciw841).

[49] ten Bosch, Q.A., Clapham, H.E., Lambrechts, L., Duong, V., Buchy, P., Althouse, B.M., Lloyd, A.L., Waller, L.A., Morrison, A.C., Kitron, U., et al. 2018 Contributions from the silent majority dominate dengue virus transmission. *PLos Pathog.* **14**, e1006965-e1006965. (doi:10.1371/journal.ppat.1006965).

[50] He, X., Lau, E.H.Y., Wu, P., Deng, X., Wang, J., Hao, X., Lau, Y.C., Wong, J.Y., Guan, Y., Tan, X., et al. 2020 Temporal dynamics in viral shedding and transmissibility of COVID-19. *Nat. Med.* **26**, 672-675. (doi:10.1038/s41591-020-0869-5).

679 [51] Ren, X., Li, Y., Yang, X., Li, Z., Cui, J., Zhu, A., Zhao, H., Yu, J., Nie, T., Ren, M., et al.
680 2020 Evidence for pre-symptomatic transmission of coronavirus disease 2019 (COVID-19) in
681 China. *Influenza Other Respi. Viruses*, 1-9. (doi:10.1111/irv.12787).
682 [52] Yanes-Lane, M., Winters, N., Fregonese, F., Bastos, M., Perlman-Arrow, S., Campbell, J.R.
683 & Menzies, D. 2020 Proportion of asymptomatic infection among COVID-19 positive persons and
684 their transmission potential: A systematic review and meta-analysis. *PLoS One* **15**.
685 (doi:10.1371/journal.pone.0241536).
686 [53] Meyerowitz, E.A., Richterman, A., Bogoch, I.I., Low, N. & Cevik, M. 2020 Towards an
687 accurate and systematic characterisation of persistently asymptomatic infection with SARS-CoV-
688 2. *The Lancet Infectious Diseases*. (doi:10.1016/ S1473-3099(20)30837-9).
689 [54] Oran, D.P. & Topol, E.J. 2020 Prevalence of Asymptomatic SARS-CoV-2 Infection: A
690 Narrative Review. *Ann. Intern. Med.* **173**, 362-367. (doi:10.7326/M20-3012).
691 [55] Klinkenberg, D., Fraser, C. & Heesterbeek, H. 2006 The Effectiveness of Contact Tracing in
692 Emerging Epidemics. *PLoS One* **1**, e12-e12. (doi:10.1371/journal.pone.0000012).
693 [56] Webb, G., Browne, C., Huo, X., Seydi, O., Seydi, M. & Magal, P. 2015 A Model of the 2014
694 Ebola Epidemic in West Africa with Contact Tracing. *PLoS Curr.* **7**.
695 (doi:10.1371/currents.outbreaks.846b2a31ef37018b7d1126a9c8adf22a).
696 [57] Davies, N.G., Kucharski, A.J., Eggo, R.M., Gimma, A., Edmunds, W.J., Jombart, T.,
697 O'Reilly, K., Endo, A., Hellewell, J., Nightingale, E.S., et al. 2020 Effects of non-pharmaceutical
698 interventions on COVID-19 cases, deaths, and demand for hospital services in the UK: a
699 modelling study. *The Lancet Public Health* **5**, E375-E385. (doi:10.1016/S2468-2667(20)30133-
700 X).
701 [58] Thompson, R.N. 2020 Epidemiological models are important tools for guiding COVID-19
702 interventions. *BMC Med.* **18**. (doi:10.1186/s12916-020-01628-4).

703 [59] Nishiura, H. & Kamiya, K. 2011 Fever screening during the influenza (H1N1-2009)
704 pandemic at Narita International Airport, Japan. *BMC Infect. Dis.* **11**, 111-111. (doi:10.1186/1471-
705 2334-11-111).
706 [60] Quilty, B.J., Clifford, S., group, C.n.w., Flasche, S. & Eggo, R.M. 2020 Effectiveness of
707 airport screening at detecting travellers infected with novel coronavirus (2019-nCoV).
708 *Eurosurveillance* **25**, 2000080-2000080. (doi:10.2807/1560-7917.ES.2020.25.5.2000080).
709 [61] Chinazzi, M., Davis, J.T., Ajelli, M., Gioannini, C., Litvinova, M., Merler, S., y Piontti, A.P.,
710 Mu, K., Rossi, L., Sun, K., et al. 2020 The effect of travel restrictions on the spread of the 2019
711 novel coronavirus (COVID-19) outbreak. *Science* **368**, 395-400. (doi:10.1126/science.aba9757).
712 [62] Dickens, B.L., Koo, J.R., Lim, J.T., Sun, H., Clapham, H.E., Wilder-Smith, A. & Cook, A.R.
713 2020 Strategies at points of entry to reduce importation risk of COVID-19 cases and reopen travel.
714 *J. Travel Med.*, taaa141-taaa141. (doi:10.1093/jtm/taaa141).
715 [63] Prem, K., Cook, A.R. & Jit, M. 2017 Projecting social contact matrices in 152 countries using
716 contact surveys and demographic data. *PLOS Computational Biology* **13**, e1005697.
717 (doi:10.1371/journal.pcbi.1005697).
718 [64] Zhang, J., Litvinova, M., Liang, Y., Wang, Y., Wang, W., Zhao, S., Wu, Q., Merler, S.,
719 Viboud, C., Vespignani, A., et al. 2020 Changes in contact patterns shape the dynamics of the
720 COVID-19 outbreak in China. *Science* **368**, 1481-1486. (doi:10.1126/science.abb8001).
721 [65] Kang, S.-J. & Jung, S.I. 2020 Age-Related Morbidity and Mortality among Patients with
722 COVID-19. *J. Infect. Chemother.* **52**, 154-164. (doi:10.3947/ic.2020.52.2.154).
723 [66] Davies, N.G., Klepac, P., Liu, Y., Prem, K., Jit, M., Pearson, C.A.B., Quilty, B.J., Kucharski,
724 A.J., Gibbs, H., Clifford, S., et al. 2020 Age-dependent effects in the transmission and control of
725 COVID-19 epidemics. *Nature Medicine* **26**, 1205-1211. (doi:10.1038/s41591-020-0962-9).

726 [67] Endo, A., Centre for the Mathematical Modelling of Infectious Diseases COVID-19 Working
727 Group, Abbott, S., Kucharski, A. & Funk, S. 2020 Estimating the overdispersion in COVID-19
728 transmission using outbreak sizes outside China [version 3; peer review: 2 approved]. *Wellcome*
729 *Open Research* **5**. (doi:10.12688/wellcomeopenres.15842.3).
730 [68] Lau, M.S.Y., Grenfell, B., Thomas, M., Bryan, M., Nelson, K. & Lopman, B. 2020
731 Characterizing superspreading events and age-specific infectiousness of SARS-CoV-2
732 transmission in Georgia, USA. *Proc. Natl. Acad. Sci. U. S. A.* **117**, 22430-22435.
733 (doi:10.1073/pnas.2011802117).
734 [69] Woolhouse, M.E.J., Dye, C., Etard, J.-F., Smith, T., Charlwood, J.D., Garnett, G.P., Hagan,
735 P., Hii, J.L.K., Ndhlovu, P.D., Quinnell, R.J., et al. 1997 Heterogeneities in the transmission of
736 infectious agents: Implications for the design of control programs. *Proceedings of the National*
737 *Academy of Sciences* **94**, 338-342. (doi:10.1073/pnas.94.1.338).
738 [70] Thompson, R.N., Hollingsworth, T.D., Isham, V., Arribas-Bel, D., Ashby, B., Britton, T.,
739 Challenor, P., Chappell, L.H.K., Clapham, H., Cunniffe, N.J., et al. 2020 Key questions for
740 modelling COVID-19 exit strategies. *Proceedings of the Royal Society B: Biological Sciences* **287**,
741 20201405. (doi:10.1098/rspb.2020.1405).
742 [71] Lloyd-Smith, J.O., Schreiber, S.J., Kopp, P.E. & Getz, W.M. 2005 Superspreading and the
743 effect of individual variation on disease emergence. *Nature* **438**, 355-359.
744 (doi:10.1038/nature04153).
745 [72] Lipsitch, M., Cohen, T., Cooper, B., Robins, J.M., Ma, S., James, L., Gopalakrishna, G.,
746 Chew, S.K., Tan, C.C., Samore, M.H., et al. 2003 Transmission Dynamics and Control of Severe
747 Acute Respiratory Syndrome. *Science* **300**, 1966-1970. (doi:10.1126/science.1086616).
748 [73] Norris, J.R. 1997 *Markov Chains (Cambridge Series in Statistical and Probabilistic*
749 *Mathematics)*. Cambridge, Cambridge University Press.

Supplementary Text

Text S1. Probability of a local outbreak

In the Methods section of the main text, we outlined an approach for deriving the probability of a local outbreak starting from a single infectious host in either the presymptomatic, symptomatic or asymptomatic classes. Here, we provide more details about that derivation. The probability of a local outbreak not occurring, starting from i presymptomatic hosts, j symptomatic hosts and k asymptomatic hosts, is denoted by $q_{i,j,k}$. If we consider the temporal evolution of (i,j,k) to be a Markov process on the state space $M = \mathbb{Z}_{\geq 0} \times \mathbb{Z}_{\geq 0} \times \mathbb{Z}_{\geq 0}$, then $q_{i,j,k}$ is the hitting probability of the state $(0,0,0)$ starting from the state (i,j,k). The vector of hitting probabilities $q^* = \{q^*_{i,j,k} \mid (i,j,k) \in M\}$ is therefore the minimal non-negative (real) solution to the following system of equations:

$q_{0,0,0} = 1$,

$q_{i,j,k} = \sum_{(l,m,n)\in M} p_{(i,j,k),(l,m,n)}\, q_{l,m,n}$ for $(i,j,k) \neq (0,0,0)$,

where $p_{(i,j,k),(l,m,n)}$ is the transition probability from state (i,j,k) to state (l,m,n) [73].

Here, minimality means that if $\hat{q} = \{\hat{q}_{i,j,k} \mid (i,j,k) \in M\}$ is another non-negative real solution, then $q^*_{i,j,k} \leq \hat{q}_{i,j,k}$ for all $(i,j,k) \in M$.

From this, equations (3), (4) and (5) in the main text are obtained. These equations may be reduced to the following quartic equation for $q_{0,0,1}$:

$$\omega_4 {q_{0,0,1}}^4 + \omega_3 {q_{0,0,1}}^3 + \omega_2 {q_{0,0,1}}^2 + \omega_1 q_{0,0,1} + \omega_0 = 0,$$

where

$\omega_4 = d(a-d)(d-c)\xi$;

$\omega_3 = cd(a-d)(1-d)\xi - bd^3(1-c)(1-\xi) + (d-c)[d-a-ad\xi + d^2(a-1+b(1-\xi)+\xi)]$;

$w_2 = c(1-d)[d-a-ad\xi + d^2(a-1+b(1-\xi)+\xi)] + (d-c)[d(d-2a-1)+2a]$;

$\omega_1 = c(1-d)[d(d-2a-1)+2a] - a(1-d)^2(d-c)$;

$\omega_0 = -ac(1-d)^3$.

The parameters a, b, c, d and ξ are as defined in the main text.

This yields four solutions for $q_{0,0,1}$ and four corresponding solutions for each of $q_{1,0,0}$ and $q_{0,1,0}$. One solution is always given by $q_{1,0,0} = q_{0,1,0} = q_{0,0,1} = 1$; the other solutions may be found numerically. As described above, we take the minimal non-negative real solution $q_{1,0,0} = q^*_{1,0,0}, q_{0,1,0} = q^*_{0,1,0}, q_{0,0,1} = q^*_{0,0,1}$, and observe that the probability of a local outbreak occurring starting from i presymptomatic hosts, j symptomatic hosts and k asymptomatic hosts is simply $1 - q_{i,j,k}$, giving the result stated in the main text.

If required, this result can be confirmed for specific model parameter values via repeated stochastic simulation of the branching process model, starting from i presymptomatic hosts, j symptomatic hosts and k asymptomatic hosts. As described in the main text, in simulations of branching process models, initial cases typically either fade out or go on to cause a local outbreak. There is a natural definition of a local outbreak as a simulation in which a large number of infections occur (see Supplementary Fig S1B). The probability of a local outbreak then corresponds to the proportion of simulations in which large numbers of infections occur.

We note here that although this is a natural way to define a local outbreak, alternative definitions exist that may be more appropriate in particular contexts. This is discussed by Thompson *et al.* (reference [41] in the main text), who consider three practically relevant definitions of an outbreak based on different criteria for measuring severity.

Text S2. Computation of steepest descent contours

The steepest descent contours shown in Fig 3A of the main text were computed using a gradient maximisation approach, in which at each point the contour direction was determined by minimising the local outbreak probability over a fixed search radius (Fig S2 A,B). Starting from ρ_1, ρ_2, at each step we considered increasing ρ_1 by an amount $\Delta\rho_1$ and increasing ρ_2 by an amount $\Delta\rho_2$ subject to the constraint $(\Delta\rho_1)^2 + (\Delta\rho_2)^2 = r^2$, where r is a small pre-specified constant. To achieve this, we scanned over the circular arc $\Delta\rho_1 = r\cos\theta\,, \Delta\rho_2 = r\sin\theta$, for $\theta \in [0, \pi/2]$ (Fig S2 A). In practice, this range was discretised into 33 search

directions evenly spaced between 0 and $\pi/2$. We then selected the pair of $\Delta\rho_1, \Delta\rho_2$ values for which the local outbreak probability evaluated at $\rho_1 + \Delta\rho_1$, $\rho_2 + \Delta\rho_2$ was minimised. The process was then repeated beginning from $\rho_{1_{new}} = \rho_1 + \Delta\rho_1$, $\rho_{2_{new}} = \rho_2 + \Delta\rho_2$ (Fig S2 B). The white line in Fig 3B, which divides the region in which increasing ρ_1 has a greater effect on the local outbreak probability from the region in which increasing ρ_2 has a greater effect on the local outbreak probability, was computed in an analogous way, with the additional restriction that we only considered the search directions $\theta = 0$ and $\theta = \pi/2$ (i.e. intensifying only surveillance of nonsymptomatic or symptomatic hosts; see Fig S2 C).

In Fig 3C, the white line represents the contour of steepest descent under the constraint that the total change in surveillance effort ($\Delta\rho_1 + \Delta\rho_2 = S$) is held constant at each step, rather than fixing the search radius $(\Delta\rho_1)^2 + (\Delta\rho_2)^2 = r^2$ as in Fig 3A. Therefore, instead of scanning over a circular arc, at each step we scan along the line $\Delta\rho_1 = s$, $\Delta\rho_2 = S - s$, where c varies in the range $[0, S]$ (Fig S2 D). Otherwise, the process is completely analogous to that described above.

Text S3. Robustness of results to parameter values used

We conducted supplementary analyses to investigate how our results are affected by varying the parameters from their baseline values given in Table 1. We performed sensitivity analyses on the values of $R_0, \xi, K_p, K_a, \gamma + \mu, \epsilon, \lambda, \nu$ and δ. For each of these, we present plots analogous to Fig 3D for six different values of the relevant parameter (Figs S3-S12). In each case we considered, our qualitative message was unchanged: whenever the maximum acceptable risk level was below a particular threshold value, the optimal strategy involved surveillance targeting both nonsymptomatic and symptomatic individuals.

Text S4. Details on computer code

All computer code was written in the MATLAB programming environment (version R2019a).

Supplementary Figures

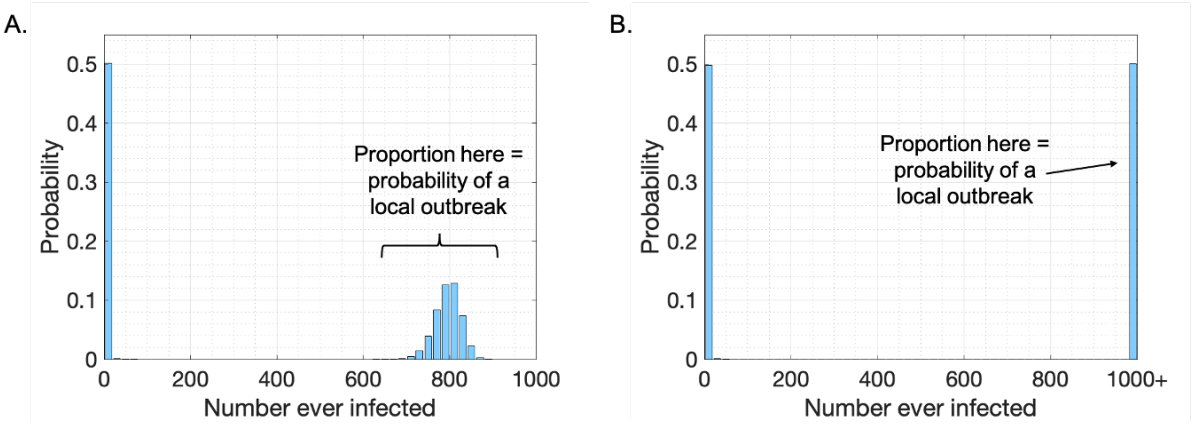

Fig S1. Illustrating the definition of the term 'local outbreak' with a simple example. A. The total number of individuals ever infected (final epidemic size) in each of 100,000 simulations of a stochastic SIR (Susceptible-Infected-Removed) model with basic reproduction number $R_0 = 2$, beginning from a single infectious host each time. Within each simulation, each event is either an infection event (with probability $\frac{R_0 S}{R_0 S+N}$) or a removal event (with probability $\frac{N}{R_0 S+N}$), and simulations are run until the pathogen fades out (I hits zero). This provides a natural partitioning between simulations that fade out quickly and those that go on to become local outbreaks. In 50% of simulations, fewer than 20 infections occurred in total (left hand peak); initial cases did not lead to sustained transmission in the population. In the remaining 50% of simulations (local outbreaks), between 620 and 900 individuals were infected in total each time. The probability of a local outbreak is then defined as the proportion of simulations for which the final epidemic size lies within this natural upper range, here equal to 0.5. B. The analogous figure to panel A, but for the branching process version of the SIR model in which depletion of susceptibles is not accounted for (i.e. $S = N$ throughout each simulation). In this model, each event is either an infection event (with probability $\frac{R_0}{R_0+1}$) or a removal event (with probability $\frac{1}{R_0+1}$), and simulations are run until either the pathogen fades out (I hits zero) or 1000 infections have occurred. The rightmost bar corresponds to simulations in which 1000 infections occurred. There is again a natural partitioning between simulations that fade out quickly and those that go on to become local outbreaks, with the probability of a local outbreak matching the equivalent value for the stochastic SIR model (panel A).

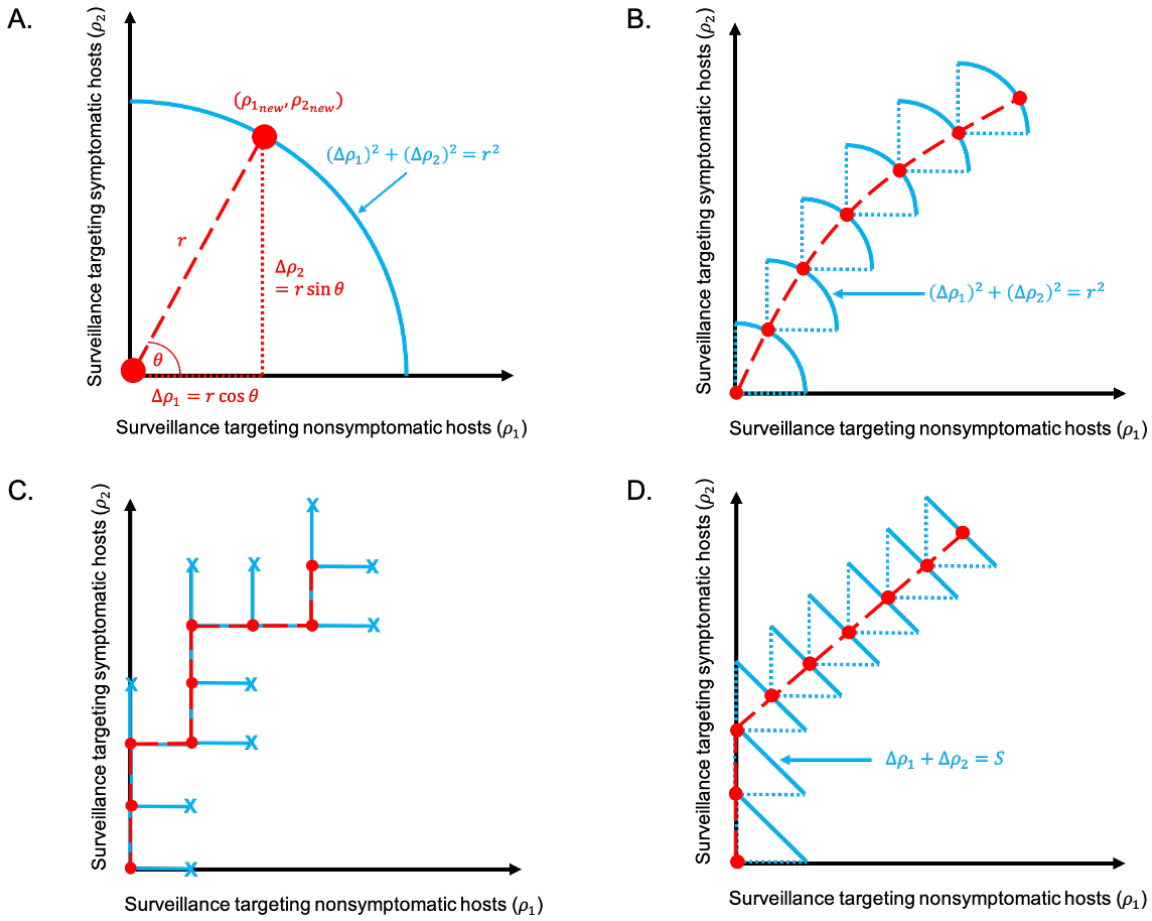

Fig S2. Computation of the steepest descent contours shown in the main text. A. To compute the steepest descent contours shown in Fig 3A of the main text, we increment ρ_1 and ρ_2 by scanning over a constant search radius $(\Delta\rho_1)^2 + (\Delta\rho_2)^2 = r^2$ (blue arc), and moving to the point $(\rho_{1_{new}}, \rho_{2_{new}})$ along that arc at which the local outbreak probability is minimised. B. The process shown in A is repeated to generate the complete contour (red dashed line). C. The analogous figure to B, in which the search direction is limited to directly to the right ($\theta = 0$) or directly upwards ($\theta = \pi/2$). This procedure is used to generate the contour in Fig 3B in the main text. D. The analogous figure to B, in which the total change in surveillance effort ($\Delta\rho_1 + \Delta\rho_2 = S$) is held constant at each step, rather than the search radius. This procedure is used to generate the contour in Figs 3C and D in the main text.

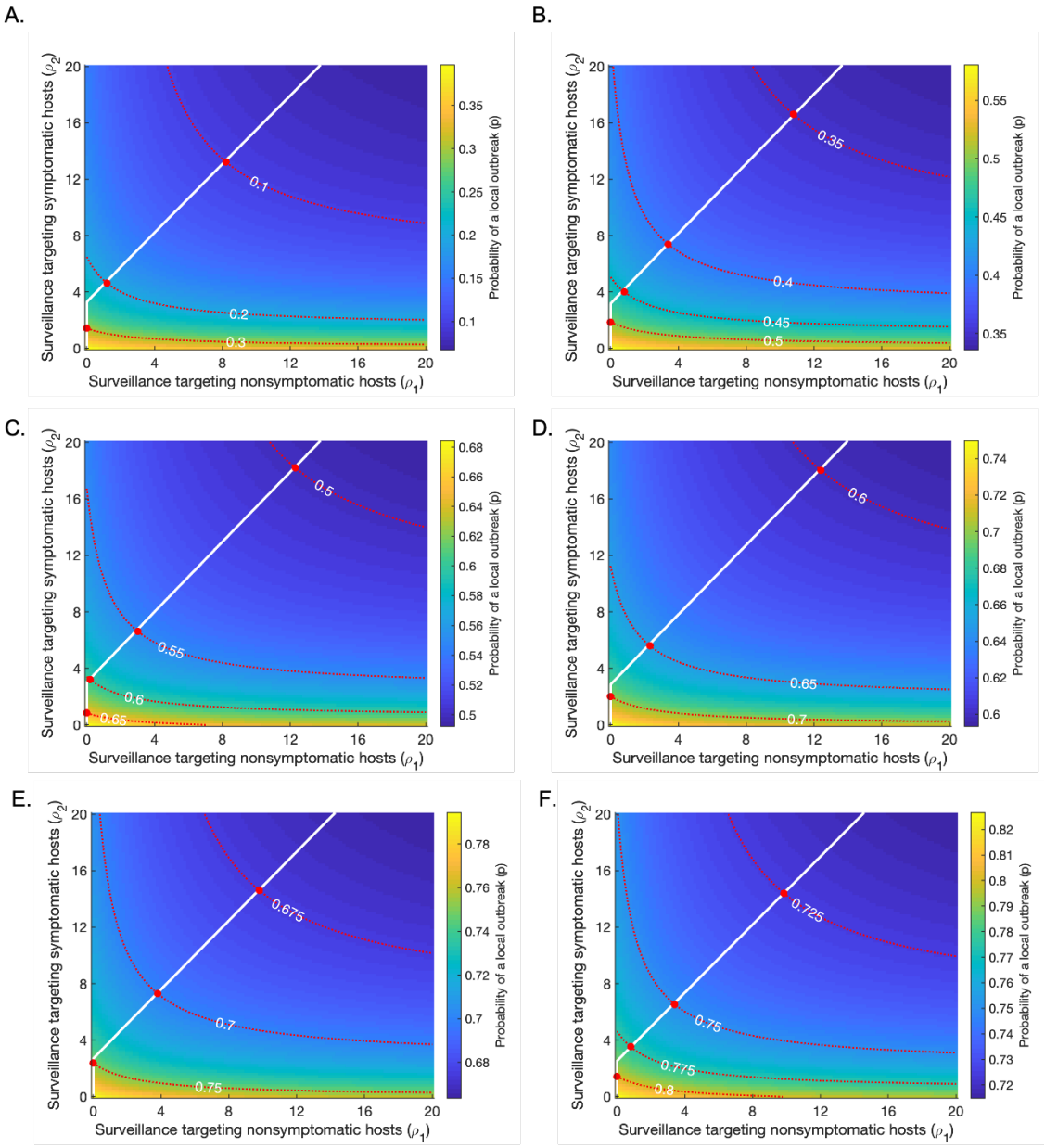

Fig S3. Varying the basic reproduction number R_0 from its baseline value ($R_0 = 3$). Plots are analogous to Fig 3D in the main text, showing strategies for minimising the surveillance effort required to achieve a pre-specified risk level (an "acceptable" local outbreak probability). Red dotted lines represent contours along which the probability of a local outbreak is constant, as labelled; red circles indicate the points along these contours at which the total surveillance effort $\rho_1 + \rho_2$ is minimised. The white line indicates the optimal strategy to follow if the pre-specified risk level is reduced. Apart from R_0 and β (which is changed in each panel to set the value of R_0), all parameters are held fixed at their baseline values given in Table 1. A. $R_0 = 1.5$. B. $R_0 = 2$. C. $R_0 = 2.5$. D. $R_0 = 3$ (baseline). E. $R_0 = 3.5$. F. $R_0 = 4$.

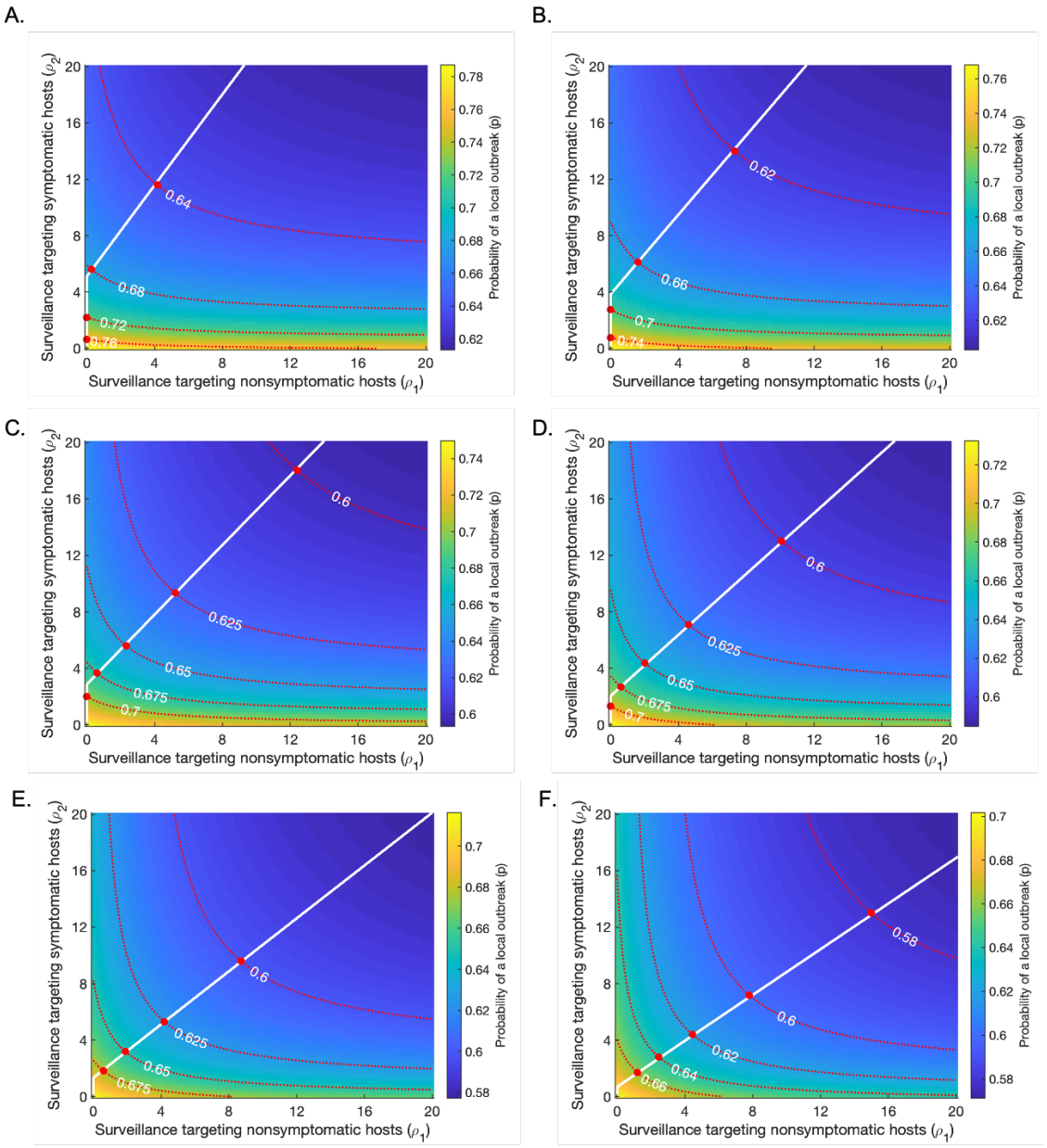

Fig S4. Varying the proportion of infections from asymptomatic infectors, ξ, from its baseline value ($\xi = 0.2$). Plots are analogous to Fig 3D in the main text, showing strategies for minimising the surveillance effort required to achieve a pre-specified risk level (an "acceptable" local outbreak probability). Red dotted lines represent contours along which the probability of a local outbreak is constant, as labelled; red circles indicate the points along these contours at which the total surveillance effort $\rho_1 + \rho_2$ is minimised. The white line indicates the optimal strategy to follow if the pre-specified risk level is reduced. Apart from ξ and β (which is changed in each panel to set $R_0 = 3$), all parameters are held fixed at their baseline values given in Table 1. A. $\xi = 0$. B. $\xi = 0.1$. C. $\xi = 0.2$ (baseline). D. $\xi = 0.3$. E. $\xi = 0.4$. F. $\xi = 0.5$.

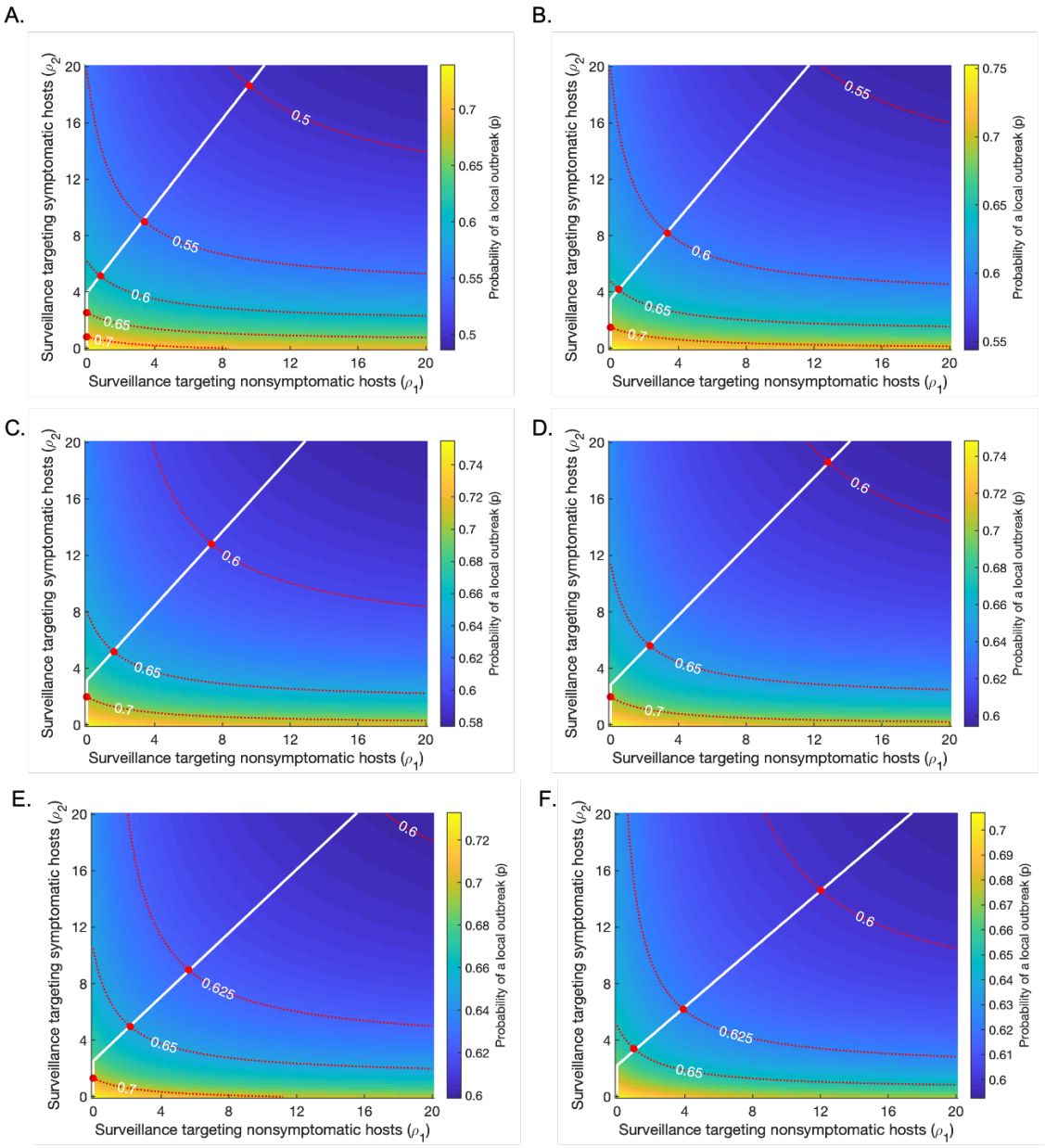

Fig S5. Varying the proportion of infections arising from presymptomatic hosts in the absence of intensified surveillance (K_p, given by expression (1) in the main text) from its baseline value ($K_p = 0.489$). In each case, the proportions of infections arising from asymptomatic and symptomatic hosts are adjusted so that they remain in the same ratio as in the baseline case. Plots are analogous to Fig 3D in the main text, showing strategies for minimising the surveillance effort required to achieve a pre-specified risk level (an "acceptable" local outbreak probability). Red dotted lines represent contours along which the probability of a local outbreak is constant, as labelled; red circles indicate the points along these contours at which the total surveillance effort $\rho_1 + \rho_2$ is minimised. The white line indicates the optimal strategy to follow if the pre-

specified risk level is reduced. Apart from K_p and K_a, as well as α and η (which are changed in each panel to set the values of K_p and K_a), and β (which is changed in each panel to set $R_0 = 3$), all parameters are held fixed at their baseline values given in Table 1. A. $K_p = 0.2$. B. $K_p = 0.3$. C. $K_p = 0.4$. D. $K_p = 0.5$. E. $K_p = 0.6$. F. $K_p = 0.7$.

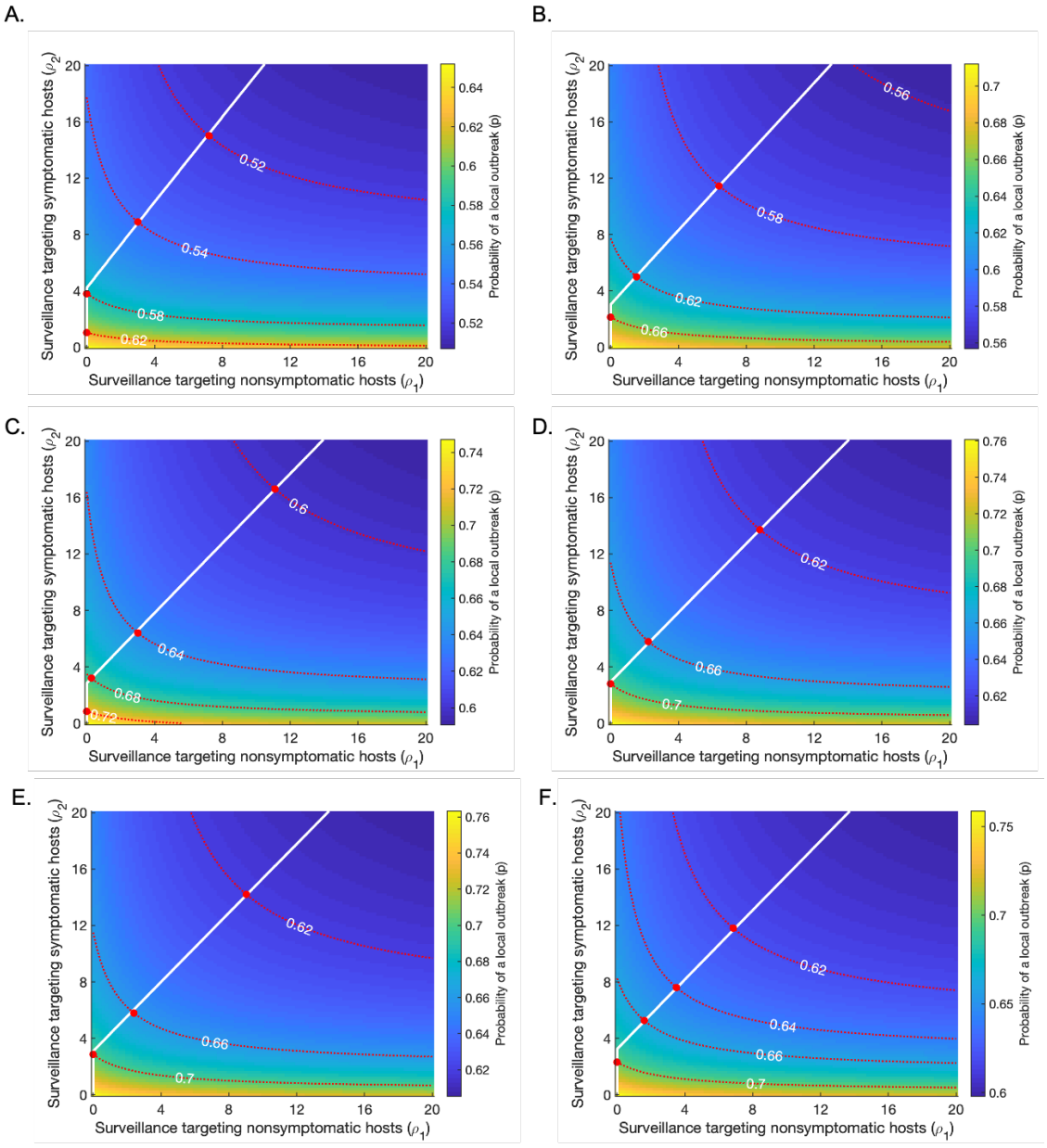

Fig S6. Varying the proportion of infections arising from asymptomatic hosts in the absence of intensified surveillance (K_a, given by expression (2) in the main text) from its baseline value ($K_a = 0.106$). In each

897 case, the proportions of infections arising from presymptomatic and symptomatic hosts are adjusted so that they
898 remain in the same ratio as in the baseline case. Plots are analogous to Fig 3D in the main text, showing
899 strategies for minimising the surveillance effort required to achieve a pre-specified risk level (an "acceptable"
900 local outbreak probability). Red dotted lines represent contours along which the probability of a local outbreak is
901 constant, as labelled; red circles indicate the points along these contours at which the total surveillance effort
902 $\rho_1 + \rho_2$ is minimised. The white line indicates the optimal strategy to follow if the pre-specified risk level is
903 reduced. Apart from K_p and K_a, as well as α and η (which are changed in each panel to set the values of K_p and
904 K_a), and β (which is changed in each panel to set $R_0 = 3$), all parameters are held fixed at their baseline values
905 given in Table 1. A. $K_a = 0.01$. B. $K_a = 0.05$. C. $K_a = 0.1$. D. $K_a = 0.15$. E. $K_a = 0.2$. F. $K_a = 0.25$.
906

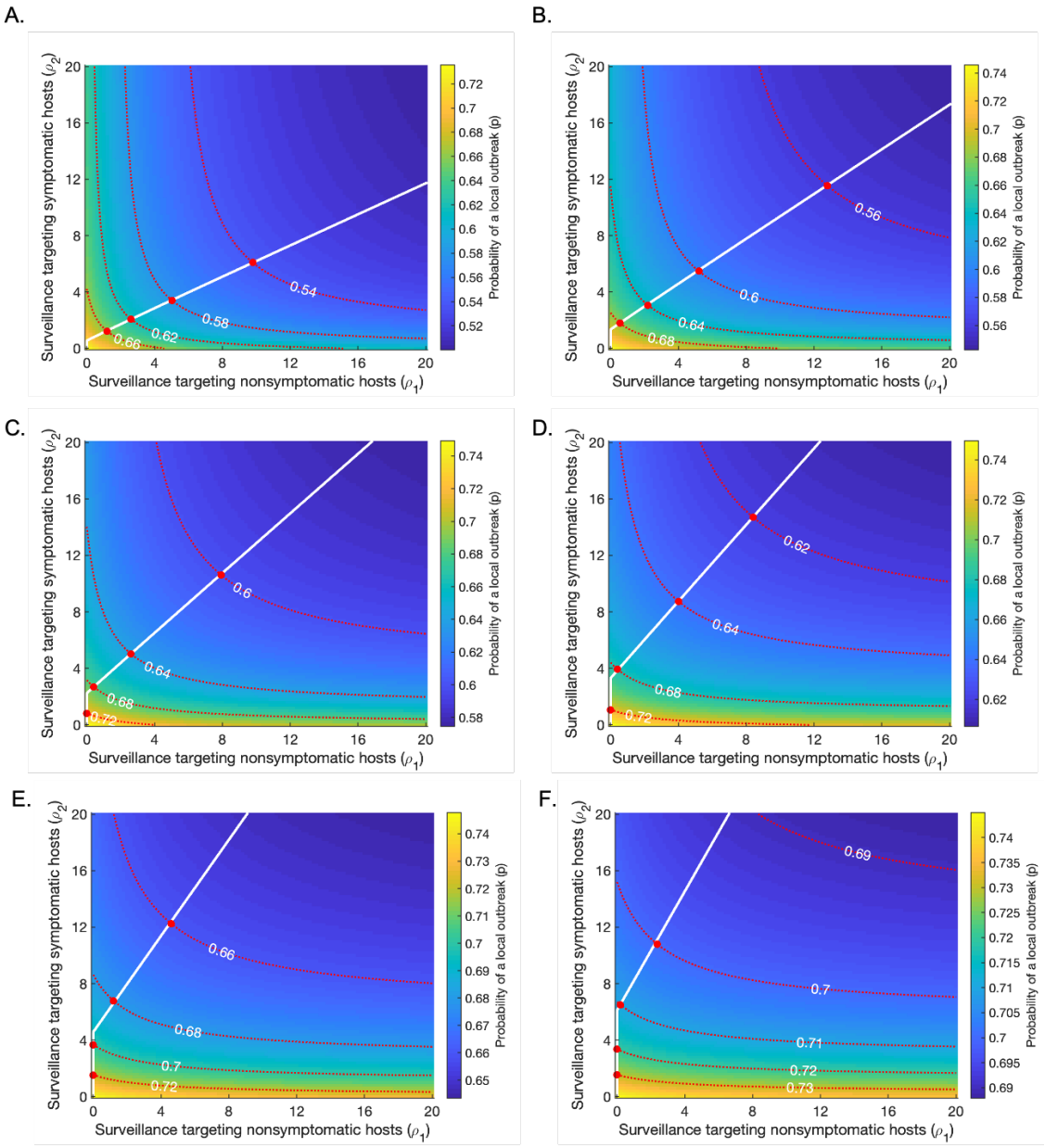

Fig S7. Varying the expected time period to isolation conditional on isolation occurring during the symptomatic period, $1/(\gamma+\mu)$, from its baseline value ($1/(\gamma+\mu) = 4.6$ days). This is achieved by varying the parameter γ, whilst holding the recovery rate of symptomatic individuals μ equal to its baseline value ($\mu = 1/8$ days^{-1}). Plots are analogous to Fig 3D in the main text, showing strategies for minimising the surveillance effort required to achieve a pre-specified risk level (an "acceptable" local outbreak probability). Red dotted lines represent contours along which the probability of a local outbreak is constant, as labelled; red circles indicate the points along these contours at which the total surveillance effort $\rho_1 + \rho_2$ is minimised. The white line indicates the optimal strategy to follow if the pre-specified risk level is reduced. Apart from γ and β (which

is changed in each panel to set $R_0 = 3$), all parameters are held fixed at their baseline values given in Table 1. A. $1/(\gamma + \mu) = 2$ days. B. $1/(\gamma + \mu) = 3$ days. C. $1/(\gamma + \mu) = 4$ days. D. $1/(\gamma + \mu) = 5$ days. E. $1/(\gamma + \mu) = 6$ days. F. $1/(\gamma + \mu) = 7$ days.

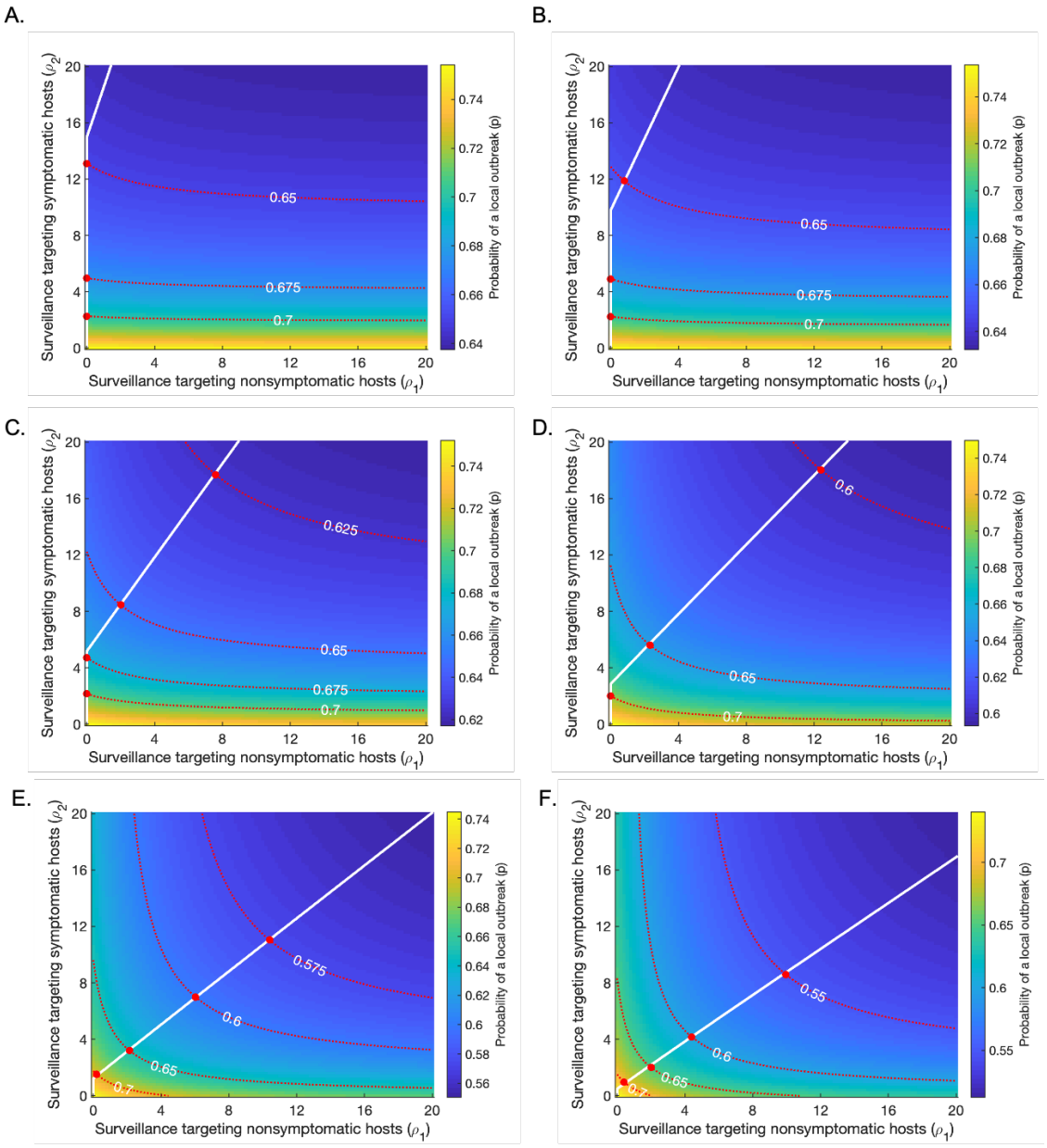

Fig S8. Varying ϵ, the relative isolation rate of nonsymptomatic individuals without intensified surveillance (compared to symptomatic individuals), from its baseline value ($\epsilon = 0.1$). Plots are analogous to Fig 3D in the main text, showing strategies for minimising the surveillance effort required to achieve a pre-specified risk level (an "acceptable" local outbreak probability). Red dotted lines represent contours along which

the probability of a local outbreak is constant, as labelled; red circles indicate the points along these contours at which the total surveillance effort $\rho_1 + \rho_2$ is minimised. The white line indicates the optimal strategy to follow if the pre-specified risk level is reduced. Apart from ϵ and β (which is changed in each panel to set $R_0 = 3$), all parameters are held fixed at their baseline values given in Table 1. A. $\epsilon = 0.01$. B. $\epsilon = 0.02$. C. $\epsilon = 0.05$. D. $\epsilon = 0.1$ (baseline). E. $\epsilon = 0.2$. F. $\epsilon = 0.3$.

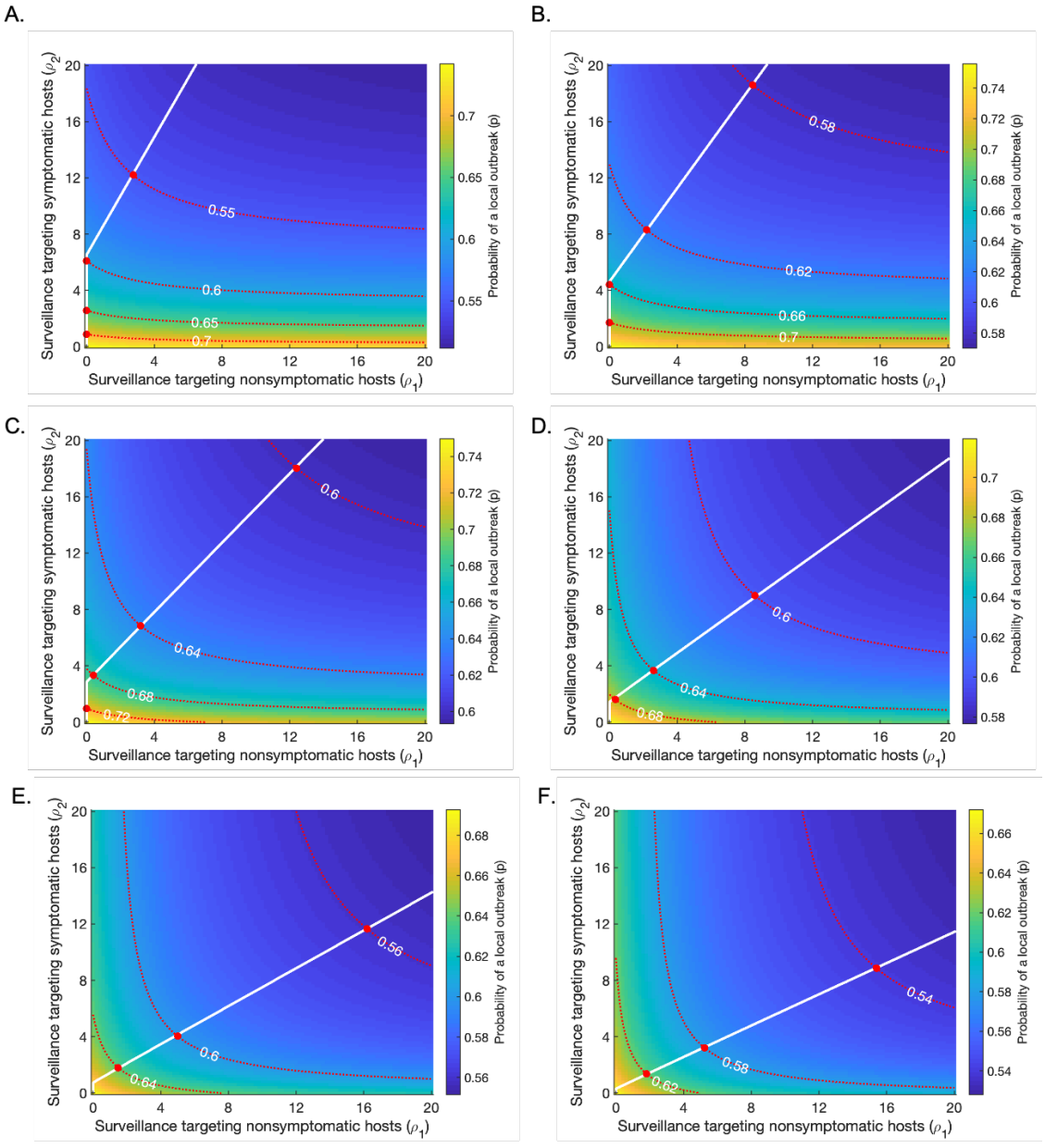

Fig S9. Varying the duration of the presymptomatic period, $1/\lambda$, from its baseline value ($1/\lambda = 0.5$ days). Plots are analogous to Fig 3D in the main text, showing strategies for minimising the surveillance effort required

934 to achieve a pre-specified risk level (an "acceptable" local outbreak probability). Red dotted lines represent
935 contours along which the probability of a local outbreak is constant, as labelled; red circles indicate the points
936 along these contours at which the total surveillance effort $\rho_1 + \rho_2$ is minimised. The white line indicates the
937 optimal strategy to follow if the pre-specified risk level is reduced. Apart from λ and β (which is changed in
938 each panel to set $R_0 = 3$), all parameters are held fixed at their baseline values given in Table 1. A. $1/\lambda = 0.5$
939 days. B. $1/\lambda = 1$ day. C. $1/\lambda = 2$ days (baseline). D. $1/\lambda = 4$ days. E. $1/\lambda = 6$ days. F. $1/\lambda = 8$ days.
940

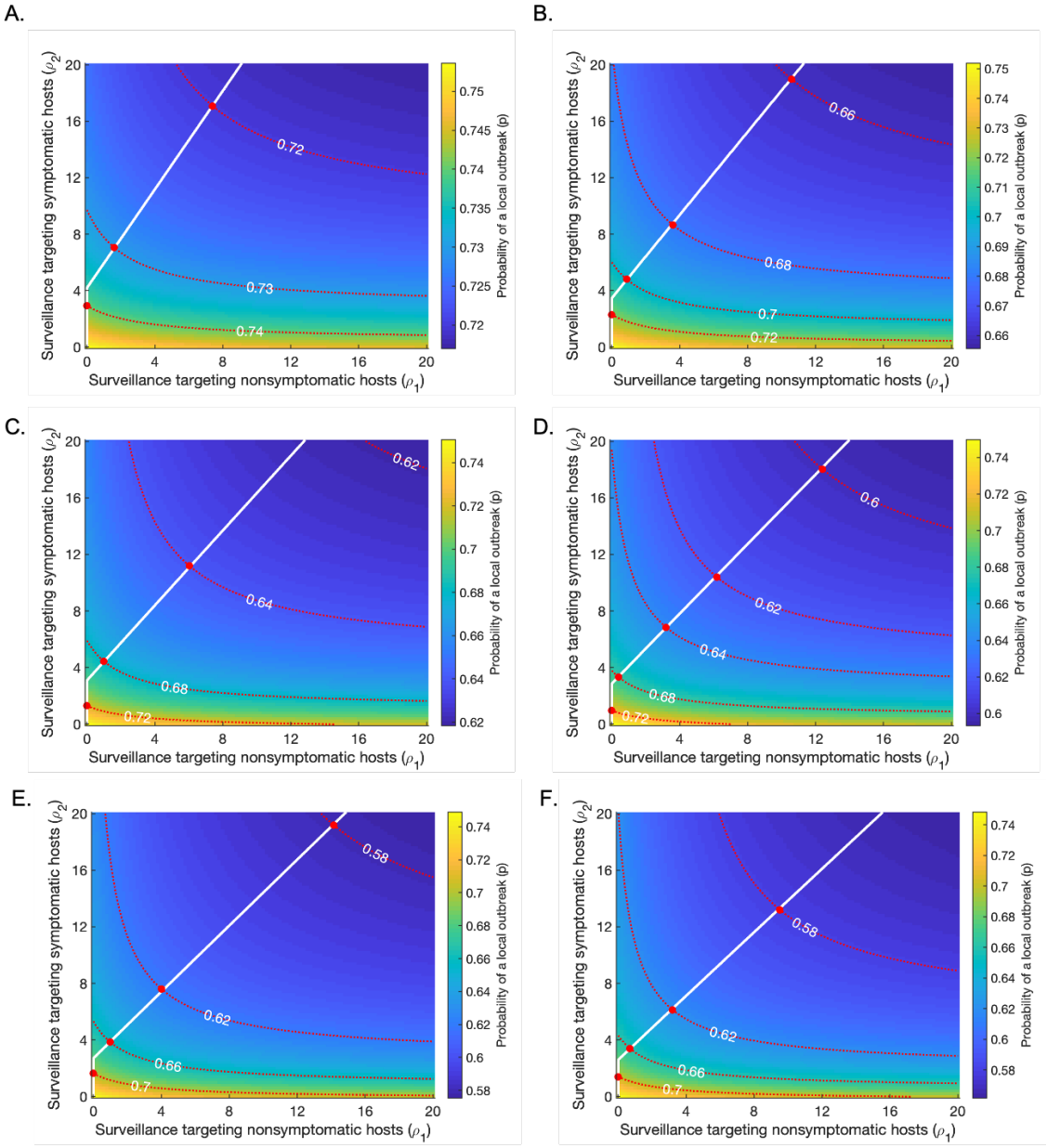

941

Fig S10. Varying the duration of the symptomatic period, $1/\mu$, from its baseline value ($1/\mu = 8$ days). The parameter γ is varied simultaneously such that $1/(\gamma + \mu)$, the expected time period to isolation conditional on isolation occurring during the symptomatic period, remains at its baseline value ($1/(\gamma + \mu) = 4.6$ days). Plots are analogous to Fig 3D in the main text, showing strategies for minimising the surveillance effort required to achieve a pre-specified risk level (an "acceptable" local outbreak probability). Red dotted lines represent contours along which the probability of a local outbreak is constant, as labelled; red circles indicate the points along these contours at which the total surveillance effort $\rho_1 + \rho_2$ is minimised. The white line indicates the optimal strategy to follow if the pre-specified risk level is reduced. Apart from μ and γ, and β (which is changed in each panel to set $R_0 = 3$), all parameters are held fixed at their baseline values given in Table 1. A. $1/\mu =$ 5 days. B. $1/\mu = 6$ days. C. $1/\mu = 7$ days. D. $1/\mu = 8$ days (baseline). E. $1/\mu = 9$ days. F. $1/\mu = 10$ days.

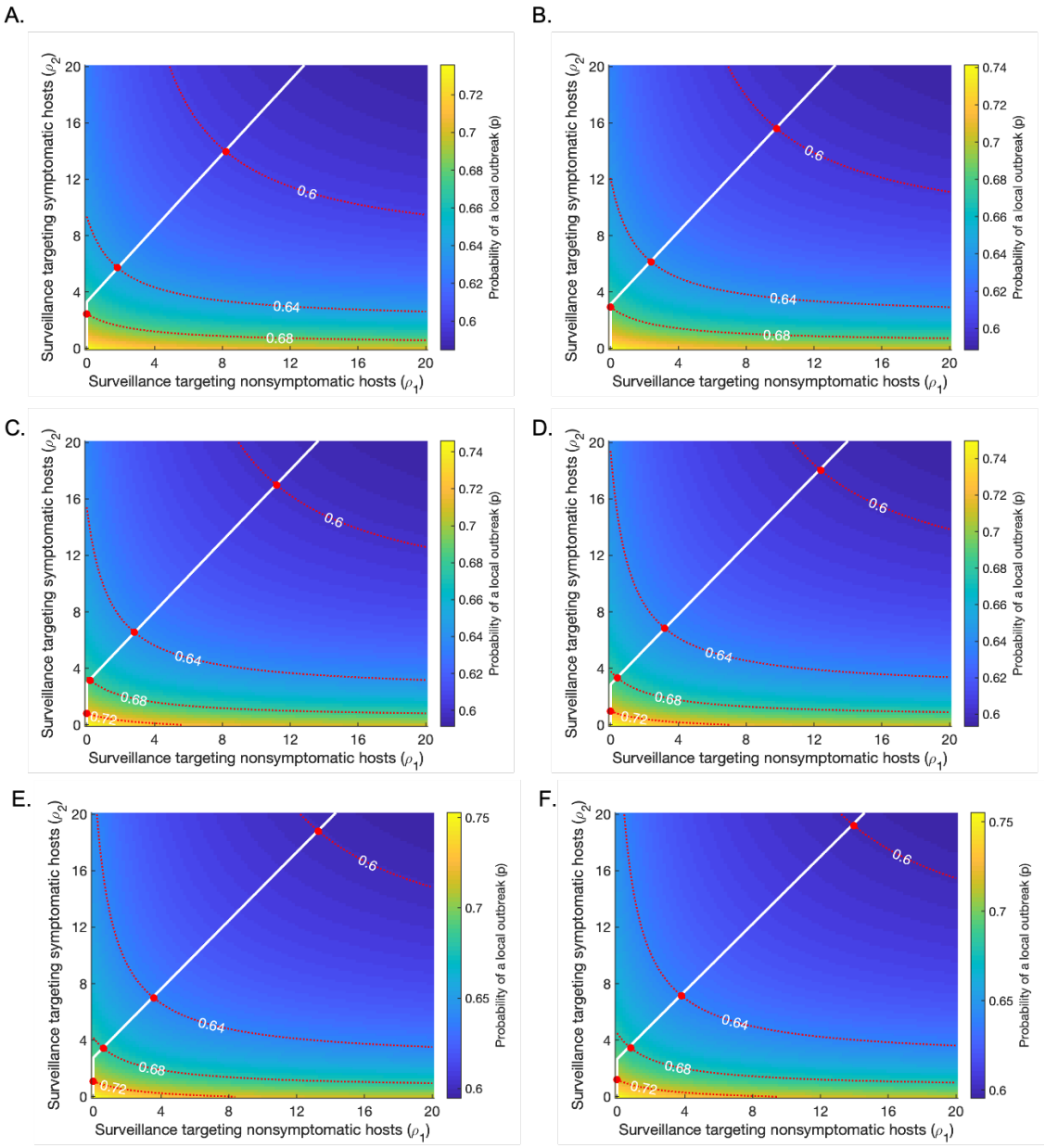

953

954 **Fig S11. Varying $1/\nu$, the duration of the asymptomatic period, from its baseline value ($1/\nu = 10$ days).**

955 Plots are analogous to Fig 3D in the main text, showing strategies for minimising the surveillance effort required

956 to achieve a pre-specified risk level (an "acceptable" local outbreak probability). Red dotted lines represent

957 contours along which the probability of a local outbreak is constant, as labelled; red circles indicate the points

958 along these contours at which the total surveillance effort $\rho_1 + \rho_2$ is minimised. The white line indicates the

959 optimal strategy to follow if the pre-specified risk level is reduced. Apart from ν and β (which is changed in

960 each panel to set $R_0 = 3$), all parameters are held fixed at their baseline values given in Table 1. A. $1/\nu = 7$

961 days. B. $1/\nu = 8$ days. C. $1/\nu = 9$ days. D. $1/\nu = 10$ days (baseline). E. $1/\nu = 11$ days. F. $1/\nu = 12$ days.

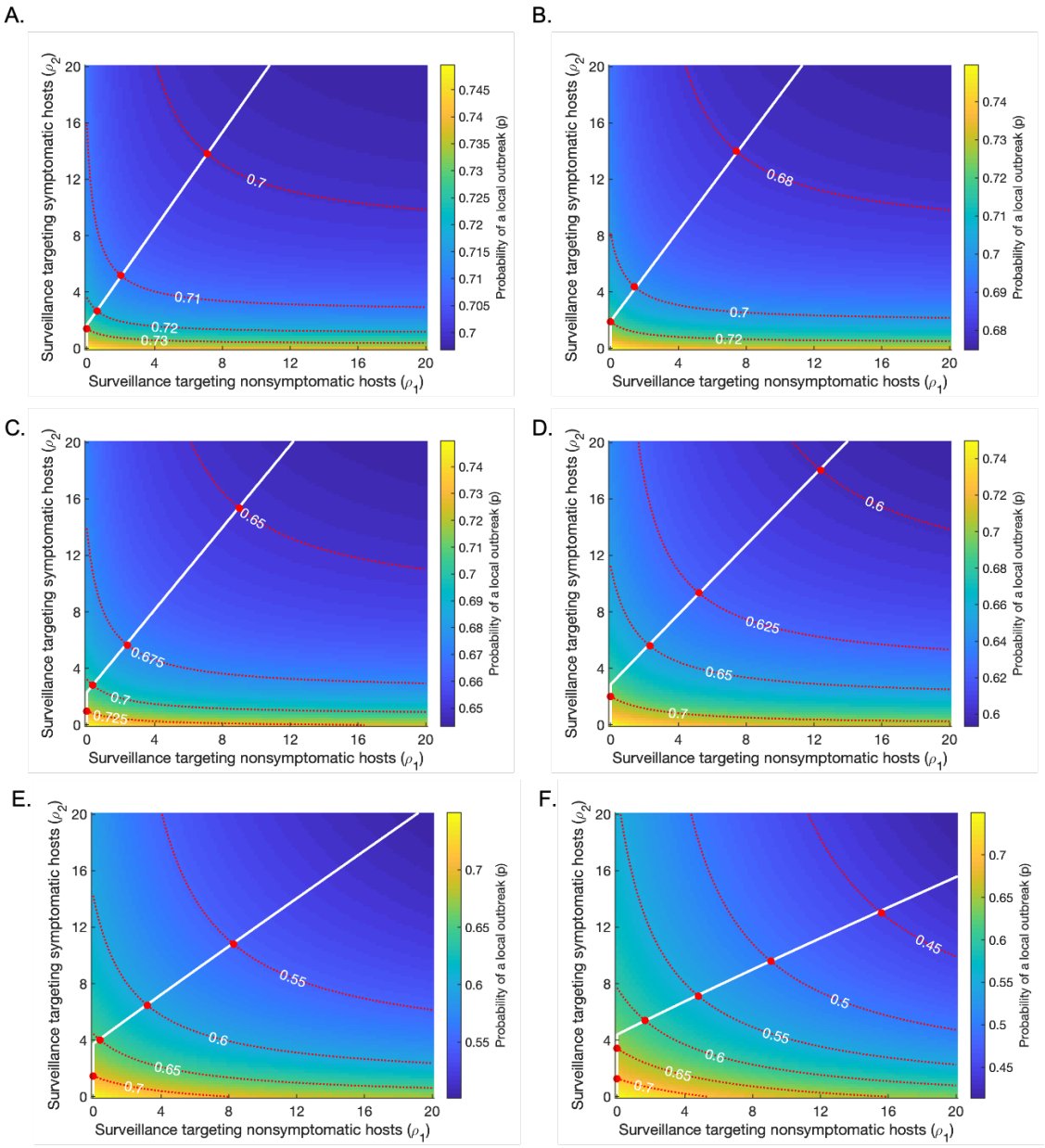

Fig S12. Varying the upper bound on the fractional reduction in the time to isolation (if no other event occurs), δ, from its baseline value ($\delta = 0.8$). Plots are analogous to Fig 3D in the main text, showing strategies for minimising the surveillance effort required to achieve a pre-specified risk level (an "acceptable" local outbreak probability). Red dotted lines represent contours along which the probability of a local outbreak is constant, as labelled; red circles indicate the points along these contours at which the total surveillance effort $\rho_1 + \rho_2$ is minimised. The white line indicates the optimal strategy to follow if the pre-specified risk level is reduced. Apart from δ, all parameters are held fixed at their baseline values given in Table 1. A. $\delta = 0.5$. B. $\delta = 0.6$. C. $\delta = 0.7$. D. $\delta = 0.8$ (baseline). E. $\delta = 0.9$. F. $\delta = 0.95$